This article has been accepted for publication in a future issue of this journal, but has not been fully edited. Content may change prior to final publication. Citation information: DOI 10.1109/TCAD.2016.2523898, IEEE Transactions on Computer-Aided Design of Integrated Circuits and Systems

Analytical Modeling and Characterization of Electromigration Effects for Multi-Branch Interconnect Trees

Hai-Bao Chen, Sheldon X.-D. Tan, *Senior Member*, Xin Huang, Taeyoung Kim, and Valeriy Sukharev

***Abstract*—Electromigration (EM) in VLSI interconnects has become one of the major reliability issues for current and future VLSI technologies. However, existing EM modeling and analysis techniques are mainly developed for a single wire. For practical VLSI chips, the elemental EM reliability unit called interconnect tree is a multi branch interconnect segment consisting of a continuously connected, highly conductive metal (Cu) lines terminated by diffusion barriers and located within the single level of metallization. The EM effects in those branches are not independent and have to be considered simultaneously. In this article, we demonstrate, for the first time, a first principle based analytical solution of this problem. We have derived the analytical expressions describing the hydrostatic stress evolution in several typical interconnect trees: the straight-line 3-terminal wires, the T-shaped 4-terminal wires and the cross-shaped 5-terminal wires. The new approach solves the stress evolution in a multi-branch tree by de-coupling the individual segments through the proper boundary conditions (BC) accounting the interactions between different branches. By using Laplace transformation technique, analytical solutions are obtained for each type of the interconnect trees. The analytical solutions in terms of a set of auxiliary basis functions using the complementary error function agree well with the numerical analysis results. Our analysis further demonstrates that using the first two dominant basis functions can lead to 0.5% error, which is sufficient for practical EM analysis.**

***Index Terms*—Electromigration, multi-branch interconnect trees, stress evolution, modeling and analysis.**

I. Introduction

Electromigration-induced reliability becomes a major design constraint in the current and future nanometer VLSI technologies. To ensure the EM signoff, conservative design rules based on the worst cases (highest possible temperature and power consumption) and simple EM model such as Black's equation can lead to significant overdesign and 2X-3X enlarged guard bands [1]. Such conservative and overdesign rules, however, will be no longer an option in current and future technologies because 3X guard band increase will significantly increase the buffer size and many other aspects of chips, which will lead to increasing currents, and hence, the cost and power of the chips. As a result, more accurate EM modeling and analysis techniques are required to ensure sufficient accuracy without sacrificing the efficiencies.

A. Physics-based EM reliability model

Existing EM model and analysis techniques mainly focus on the simple straight line interconnect with two-line end terminals. However, a practical integrated circuit layout often has interconnects with more complex, multi-branch structures. The EM-induced stress evolutions in those branches are not independent and they have to be considered simultaneously [2] [3]. Currently employed Blech limit [4] (for the out filtration of immortal segments) and Black's equation [5] (for calculating MTTFs for segments characterized by known current densities and temperatures) are subjects of the hard criticism [6] [7]. Across-die variation of residual stress makes the Blech's "critical product" to be layout-dependent variables rather than experimentally determined constants. The dependency of the Black's activation energy on the current density and temperature makes rather controversial the widely accepted methodology of calculating the MTTF at use condition. It is so because conventionally, the use activation energy and current density exponent are assumed to be the same as those determined at the stressed (accelerated) condition, characterized by high current densities and elevated temperatures.

Recently some physics-based EM analysis methods for the TSV and power grid networks have been proposed based on solving the basic mass balance equations [8]. Since these proposed methods solve the basic mass balance equations using the finite element method, they can only solve very small structures such as one TSV. Complicated look-up table or models have to be built for different TSVs and wire segments for full-chip power grid analysis at reduced accuracy. To mitigate this problem, a novel compact physics-based EM model was proposed recently in [9] [10]. It is based on the solution of the diffusion-like continuity equation describing the kinetics of hydrostatic stress evolution [11]. Although the new EM model has been extended to deal with a multiple branch tree based on the projected steady-state stress, it still cannot provide the evolution of the hydrostatic stress, which ultimately determines the failures for multi-branch interconnect wires.

To further illustrate this, Fig. 1 shows distributions of the current density and hydrostatic stress evolved in the three

Hai-Bao Chen is with Department of Micro/Nano-electronics, Shanghai Jiao Tong University, Shanghai 200240, China. Sheldon X.-D. Tan and Xin Huang are with Department of Electrical and Computer Engineering, University of California, Riverside, CA 92521, USA. Taeyoung Kim is with Department of Computer Science and Engineering, University of California, Riverside, CA 92521, USA. Valeriy Sukharev is with Mentor Graphics Corporation, Fremont, CA 94538, USA. (email: haibaochen@sjtu.edu.cn; stan@ece.ucr.edu; xhuan009@ucr.edu;tkim049@cs.ucr.edu;Valeriy_Sukharev@mentor.com).

This work is supported in part by NSF grants under No. CCF-1255899, in part by NSF Grant under No. CCF-1527324, in part by Semiconductor Research Corporation(SRC) Grant under No. 2013-TJ-2417, in part by a 985 research fund from Shanghai Jiao Tong University, and in part by NSFC grant under No. 20873999.

Copyright (c) 2015 IEEE. Personal use of this material is permitted. However, permission to use this material for any other purposes must be obtained from the IEEE by sending an email to pubs-permissions@ieee.org.

0278-0070 (c) 2015 IEEE. Personal use is permitted, but republication/redistribution requires IEEE permission. See http://www.ieee.org/publications_standards/publications/rights/index.html for more information.

This article has been accepted for publication in a future issue of this journal, but has not been fully edited. Content may change prior to final publication. Citation information: DOI 10.1109/TCAD.2016.2523898, IEEE Transactions on Computer-Aided Design of Integrated Circuits and Systems

terminals interconnect tree loaded with DC currents. Electrons inflow the upper-level metal line through the most left and middle upstream vias and outflow to the lower-level metal line through the right downstream via. The steady state hydrostatic stress distribution, which was obtained from the solution of the linked partial differential equations describing the major physics of the EM phenomenon, [12], with the FEA tool COMSOL [13], demonstrates the two-slope stress distribution resulted by the intra-branch atom diffusion. It is clear that this stress distribution can be explained by redistribution of the atoms among both the branches of the tree. Tree decomposition on two independent segments will never explain this type of stress distribution [14]. Closed-form analytical description of the distribution of hydrostatic stress caused by EM-induced redistribution of atoms inside an interconnect tree, which is needed for determination of the potential locations for void nucleation, was the major motivation for the reported work.

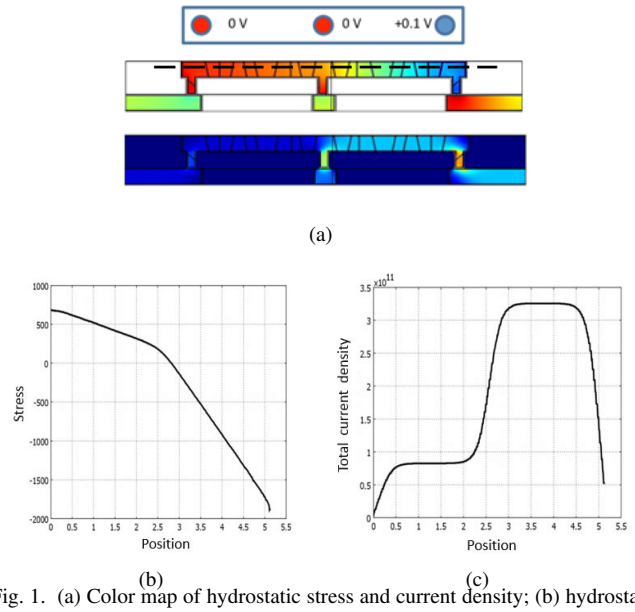

(a) (b) (c)

Fig. 1. (a) Color map of hydrostatic stress and current density; (b) hydrostatic stress along the top metal line; (c) current density distributions.

B. Related works

Many, mostly experimental studies of the EM-induced degradation of the multi-branch interconnects were reported in the literature. Vairagar *et al.* studied the dependence of EM-induced failure in a 3-terminal Cu wire on the electric current configuration in adjoining interconnect segments and provided direct evidence of the peculiar EM behavior, [15]. Experimental characterization of the reliability of dual-damascene Cu interconnect tree structures consisting of straight contact-to-contact lines has been analyzed in [16]–[18]. However, it did not give a unified analytic form to model the 3-terminal interconnect trees which strongly depend on the correlated stress evolution in neighboring segments. In [19], the effects of EM in a 3-terminal L-shaped interconnect tree were studied by using a numerical simulation technique based on solution of the one-dimensional Korhonen's equation, [11]. An analytic model for the stress evolution in the star-like tree represented by semi-infinite segments with known current densities connected at the central node has been developed in [20]. In order to implement critical threshold design rules of EM reliability, a nodal analysis technique for computing the steady-state EM-induced stress was proposed in [21]. The nodal analysis technique is an approximate method for calculating the node voltages at the ends of the interconnect segments extracted from the larger interconnect network. In [22], a systematic study of Blech effect-based model for EM in complex structures including the effect of adjacent segments has been made, but transient analysis has not been performed on this model.

In this work, we propose, for the first time, an accurate and first principle based analytic model for calculating the hydrostatic stress evolution in the finite multi-branch interconnect trees during the void nucleation phase. An ultimate goal is a capability to predict all suspicious locations inside interconnect where void can be nucleated. A well-known steady state analysis of the hydrostatic stresses distribution across the tree can provide just potential locations for void nucleation, where these stresses exceed the critical one. In reality, when the stress evolution kinetics is considered, these void nucleation site locations could be quite different. We have derived the analytical expressions describing the hydrostatic stress evolution in several typical interconnect trees: the straight-line 3-terminal wires, the T-shaped 4-terminal wires and the cross-shaped 5-terminal wires. This new approach solves the stress evolution in a multi-branch tree by decoupling the individual segments through the proper BC accounting the interactions between different branches. By using Laplace transformation technique, analytical solutions are obtained for each tree. The analytical solutions then are obtained in terms of set of auxiliary basis functions using the complementary error function. The employed transient analysis is a part of the dynamical analysis of the EM-induced IR-drop degradation. Those analytical EM models agree well with COMSOL simulation results. Furthermore, we demonstrate that employing just the first dominant basis function can lead to less than 4 % error and by using the first two basis functions the error doesn't exceed 0.5%, which is sufficient for practical EM analysis.

The rest of this article is organized as follows. Section II describes the existing analytical expression for the stress evolution in the single confined metal line with the blocking BC. In Section III, we present our analytical solutions by using the Laplace transformation technique for the straight-line 3-terminal wire, the T-shaped 4-terminal wire and the cross-shaped 5-terminal wire. In Section IV, we show the segment length effect in EM-induced stress evolution by using the proposed analytical method. Experimental results for a number of benchmark examples are provided in Section V. Concluding remarks are drawn in Section VI. The details of the mathematical derivation of the analytical EM analysis for the T-shaped 4-terminal interconnect tree and the cross-shaped 5-terminal interconnect tree are presented in the appendix.

0278-0070 (c) 2015 IEEE. Personal use is permitted, but republication/redistribution requires IEEE permission. See http://www.ieee.org/publications_standards/publications/rights/index.html for more information.

This article has been accepted for publication in a future issue of this journal, but has not been fully edited. Content may change prior to final publication. Citation information: DOI 10.1109/TCAD.2016.2523898, IEEE Transactions on Computer-Aided Design of Integrated Circuits and Systems

II. The Dynamic Stress Evaluation for a Single Segment Wire

Before we present our analytical solutions to the partial differential equation (PDE) describing the stress evolution in multi-branch interconnect trees, let us review the basic hydrostatic stress evolution taking place in a single segment wire loaded with the constant electric current.

For a one dimensional metal wire, the stress evolution $\sigma(t)$ caused by EM effects is well described by the following diffusion-like equation [11]:

$$\frac{\partial \sigma(x,t)}{\partial t} = \frac{\partial}{\partial x}[\kappa(\frac{\partial \sigma(x,t)}{\partial x} + G)], \tag{1}$$

where $\kappa = \frac{D_a B \Omega}{kT}$ is the "stress" diffusivity and $G = \frac{Eq^*}{\Omega}$ is the EM driving force, D_a is the effective atomic diffusion coefficient,

$$D_a = D_0 \exp(-\frac{E_a}{kT}). \tag{2}$$

Here, D_0 is the pre-exponential factor, E_a is the activation energy, B is the effective bulk modulus, Ω is the atomic volume, k is Boltzmann's constant, T is the absolute temperature, E is the electric field, and q^* is the effective charge. The electric field E can be replaced by the product of the resistivity ρ times the current density j, i.e., $E = \rho j$. The effective charge $q^* = |Z^*|e$ is a known quantity, where e is the elementary charge and Z^* is the effective charge number. As a result, driving force G can be re-written as $G = \frac{\rho j |Z^*| e}{\Omega}$. To facilitate the comprehension of this paper, we summarize the major notations in Table I.

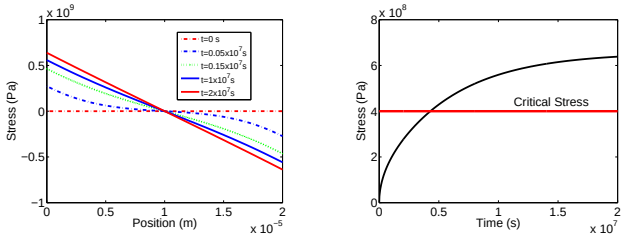

(a) (b)

Fig. 2. (a) The EM-induced stress development and distribution along a single metal wire; (b) the stress development at the cathode node.

Fig. 2 shows the stress development over time in a metal line computed by COMSOL. Fig. 2(a) shows that tensile (the positive) stress will be developed over time at the cathode node (left node) and compressive (the negative) stress will be developed at the anode node (right node). The stress changes sign in the middle of the wire. The built-up stress (its gradient) will serve as the counter-force for atomic flux. It was agreed that development of the so-called critical stress σ_{crit} should be used as a condition for a void nucleation. Indeed, due to a huge activation energy a void cannot be nucleated by, for example, vacancy agglomeration even when the stress is big. At the same time different natural flaws such as micro cracks, small process induced cavities (pores), dislocation gladding induced steps, etc. usually preexist in metal. The classical model of the homogeneous nucleation, [23], says that a cavity located in the metal, loaded with the hydrostatic tensile stress

TABLE I
Notations and Typical Value in Our Transient Simulation

Term	Typical value	Description
ρ	3e-8$\Omega\cdot$ m	Electrical resistivity
e	1.60e-19C	Electric charge
Z^*	10	Effective valence charge
Ω	8.78e-30 m^3	Atomic volume
k	1.38e-23J/K	Boltzmann constant
B	1e11Pa	Back flow stress modular
D_0	5.2e-5m^2/ s	Self-diffusion coefficient
E_a	1.1eV	Activation energy
σ_T	400MPa	Thermal stress
j	From simulation	Current density
T	From simulation	Absolute temperature
σ	From simulation	Electromigration stress

σ, can either shrink or enlarge depending on the original cavity size R. In the very rough approximation, which we use for illustrative purposes, if $R < R_c = 2\gamma/\sigma$, where γ is the cavity surface energy per unit area, the cavity will shrink to reduce the free energy of the system represented by the metal with cavity; if $R > R_c$, the cavity will enlarge to reduce this energy. Thus, assuming that the preexisting cavities are of the $5-10nm$ size, we can estimate the critical stress level of $\sigma \approx 200-500MPa$ when $\gamma = 1N/m^2$. It means, if stress exceeds the critical level then the preexisting cavities of the corresponding sizes start to grow. Rate of this growth is determined by the atomic diffusion, i.e. is pretty slow. We can see from Fig. 2(b) that if the largest stress at the cathode node exceeds the critical stress, then the growing voids will be generated. If the stress development enters a steady state (atomic diffusion stops) before it reaches the critical stress, the wire will become immortal.

Eq. (1) can have different closed-form solutions with different BC. Following Korhonen [11], we assume through in the rest of the paper that the diffusivity-like parameter κ does not depend on stress, and hence, on time. For the blocking BC, the atomic flux is blocked at both line ends $x = 0$ and $x = L$, i.e., $J(0,t) = J(L,t) = 0$ where $J(x,t) = \frac{D_a}{\Omega kT}(\frac{\partial \sigma(x,t)}{\partial x} + G)$. Following [11], the stress evolution in the line can be described as

$$\sigma(x,t,\kappa,G) = \sigma_T + GL\{\frac{1}{2} - \frac{x}{L} - 4\sum_{n=0}^{\infty} \frac{\cos((2n+1)\pi\frac{x}{L})}{(2n+1)^2\pi^2 \exp((2n+1)^2\pi^2\frac{\kappa t}{L^2})}\}, \tag{3}$$

where σ_T is the pre-existing residual stress due to a thermal process. An ultimate target of the existing EM modeling approaches is prediction of the void nucleation time, i.e. the instance in time when the stress developed in the line has reached the critical stress [24]. To derive the closed-form expression, one can keep the slowest decaying term of the infinite series in (3) to obtain the approximate estimation for stress at the line cathode end ($x = 0$) as

$$\sigma(t,T,j) \approx \sigma_T + GL(\frac{1}{2} - \frac{1}{2\exp\{\frac{D_a B \Omega t}{L^2 kT}\}}). \tag{4}$$

As a result, when $\sigma(t,T,j) \geq \sigma_{crit}$, the nucleation time t_{nuc}

0278-0070 (c) 2015 IEEE. Personal use is permitted, but republication/redistribution requires IEEE permission. See http://www.ieee.org/publications_standards/publications/rights/index.html for more information.

This article has been accepted for publication in a future issue of this journal, but has not been fully edited. Content may change prior to final publication. Citation information: DOI 10.1109/TCAD.2016.2523898, IEEE Transactions on Computer-Aided Design of Integrated Circuits and Systems

can be computed in an analytical form as below

$$t_{nuc} = \frac{L^2 kT}{D_a B\Omega} \ln\{\frac{\frac{\rho j|Z^*|eL}{2\Omega}}{\sigma_T + \frac{\rho j|Z^*|eL}{2\Omega} - \sigma_{crit}}\}. \quad (5)$$

III. New analytical models for multi-branch interconnect tree

In this section, we present our analytical solution to the multi-branch interconnect trees. We discuss three cases: the straight-line 3-terminal interconnect tree, the T-shaped 4-terminal interconnect tree, and the cross-shaped 5-terminal interconnect tree as they are commonly seen in many practical VLSI wiring for a single metal layer. In this work the tree is defined as an elemental EM reliability unit consisting of continuously connected highly conductive metal segments lying within one layer of metallization and surrounded by the diffusion barriers (Ta/TaN liners and Si(C)N dielectric barrier). In the general case the tree has more than one termination branch. In this section we focus on the three cases, corresponding to different types of trees, regarding the derivation of exact analytical solutions and approximate expressions for the hydrostatic stress evaluation in the EM void nucleation phase.

A. Straight-line 3-terminal interconnect tree

For multi-branch interconnect tree, EM-induced stress evolution in nucleation and growth phases is still governed by the Korhonen's equation [11]. But it is a difficult task to solve simultaneously the Korhonen's equation for all the branches. One viable approach is to break the multi-branch interconnect tree into a number of simple single-segment wires in a way that we can apply the Korhonen's equation for each segment. At the joints of two connected wire segments, the stress value must be continuous as well as the atomic flux. It should be noted that the last condition is valid in the case of equal segment widths, which is analyzed below. Also, note that the current densities at the boundaries may not be continuous, but must meet the Kirchhoff's circuit law.

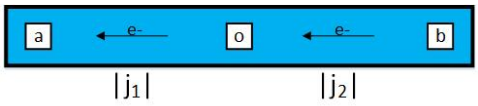

Fig. 3. The straight-line 3-terminal interconnect tree.

We first analyze the 3-terminal interconnect tree with two segments with the current flow directions as showed in Fig. 3. The current densities in the two segments may not be the same, which will be determined by the rest of the circuit. For the two segments, we have the following two diffusion equations based on the Korhonen model [11]:

$$\begin{aligned}\frac{\partial \sigma_1(x,t)}{\partial t} &= \frac{\partial}{\partial x}[\kappa_1(\frac{\partial \sigma_1(x,t)}{\partial x} + G_1)], \\ &\qquad \texttt{in } -L < x < 0,\ t > 0, \\ \frac{\partial \sigma_2(x,t)}{\partial t} &= \frac{\partial}{\partial x}[\kappa_2(\frac{\partial \sigma_2(x,t)}{\partial x} + G_2)], \\ &\qquad \texttt{in } 0 < x < L,\ t > 0.\end{aligned} \quad (6)$$

For the void nucleation phase, the hydrostatic stresses in the two segments will interplay with each other, which is reflected in the BC:

$$\begin{aligned}&\kappa_1(\frac{\partial \sigma_1(x,t)}{\partial x} + G_1) = 0,\ \texttt{at } x = -L,\ t > 0, \\ &\sigma_1(x,t) = \sigma_2(x,t),\ \texttt{at } x = 0,\ t > 0, \\ &\kappa_1(\frac{\partial \sigma_1(x,t)}{\partial x} + G_1) = \kappa_2(\frac{\partial \sigma_2(x,t)}{\partial x} + G_2), \\ &\qquad \texttt{at } x = 0,\ t > 0, \\ &\kappa_2(\frac{\partial \sigma_2(x,t)}{\partial x} + G_2) = 0,\ \texttt{at } x = L,\ t > 0.\end{aligned} \quad (7)$$

The second equation in (7) means that stresses at the boundary need to be continuous. The third one indicates that the atom flux is also continuous at the boundary. The initial conditions (IC) of the equations are as follows:

$$\begin{aligned}&\sigma_1(x,t) = 0,\ \texttt{for } t = 0, \texttt{in } -L < x < 0, \\ &\sigma_2(x,t) = 0,\ \texttt{for } t = 0, \texttt{in } 0 < x < L,\end{aligned} \quad (8)$$

which basically says that there is no stress anywhere in the whole tree at $t = 0$. With the given boundary and initial conditions, it turns out that we can use the Laplace transform technique to obtain the exact analytical solution for the stresses in these two segments, which are expressed as infinite series of some basis functions.

Starting with the function $\sigma(x,t)$ of time and space coordinates, the Laplace transform of $\sigma(x,t)$ can be defined as $\hat{\sigma}(x,s) = \int_0^{+\infty} e^{-st}\sigma(x,t)dt$. This new function has several important properties which will turn out to be convenient for purposes of solving the diffusion equations (6) with the BC (7) and the IC (8). The Laplace transform technique has been used to calculate the hydrostatic stress evolution at the intersection of a semi-infinite interconnect, [18] [20]. However, they did not give an exact closed-form expression of the stress evolution of this type of interconnect if each segment has finite length. Using this Laplace transform for (6) with the IC (8), we get the ordinary differential equations

$$\begin{aligned}\frac{d^2\hat{\sigma}_1(x,s)}{dx^2} &= \frac{s}{\kappa_1}\hat{\sigma}_1(x,s),\ -L < x < 0, \\ \frac{d^2\hat{\sigma}_2(x,s)}{dx^2} &= \frac{s}{\kappa_2}\hat{\sigma}_2(x,s),\ 0 < x < L.\end{aligned} \quad (9)$$

Solution of these equations provides:

$$\begin{aligned}\hat{\sigma}_1(x,s) &= A_{1,I}e^{\sqrt{\frac{s}{\kappa_1}}x} + B_{1,I}e^{-\sqrt{\frac{s}{\kappa_1}}x}, \\ \hat{\sigma}_2(x,s) &= A_{2,I}e^{\sqrt{\frac{s}{\kappa_2}}x} + B_{2,I}e^{-\sqrt{\frac{s}{\kappa_2}}x}.\end{aligned} \quad (10)$$

We will need to calculate the undetermined coefficients $A_{1,I}$, $A_{2,I}$, $B_{1,I}$, and $B_{2,I}$ so that the corresponding solutions satisfy the BC (7). Using the Laplace transform again, we get

$$\begin{aligned}&\frac{d\hat{\sigma}_1(x,s)}{dx} + \frac{G_1}{s} = 0,\ \texttt{at } x = -L, \\ &\sigma_1(x,s) = \sigma_2(x,s),\ \texttt{at } x = 0, \\ &\kappa_1(\frac{d\hat{\sigma}_1(x,s)}{dx} + \frac{G_1}{s}) = \kappa_2(\frac{d\hat{\sigma}_2(x,s)}{dx} + \frac{G_2}{s}),\ \texttt{at } x = 0, \\ &\frac{d\hat{\sigma}_2(x,s)}{dx} + \frac{G_2}{s} = 0,\ \texttt{at } x = L.\end{aligned} \quad (11)$$

0278-0070 (c) 2015 IEEE. Personal use is permitted, but republication/redistribution requires IEEE permission. See http://www.ieee.org/publications_standards/publications/rights/index.html for more information.

This article has been accepted for publication in a future issue of this journal, but has not been fully edited. Content may change prior to final publication. Citation information: DOI 10.1109/TCAD.2016.2523898, IEEE Transactions on Computer-Aided Design of Integrated Circuits and Systems

Substituting the expressions $\hat{\sigma}_1(x,s)$ and $\hat{\sigma}_2(x,s)$ from (10) into (11), we obtain

$$\begin{bmatrix} \frac{a_1}{d_1} & -a_1 d_1 & 0 & 0 \\ 0 & 0 & a_2 d_2 & -\frac{a_2}{d_2} \\ \kappa_1 a_1 & -\kappa_1 a_1 & -\kappa_2 a_2 & \kappa_2 a_2 \\ 1 & 1 & -1 & -1 \end{bmatrix} \begin{bmatrix} A_{1,I} \\ B_{1,I} \\ A_{2,I} \\ B_{2,I} \end{bmatrix} = \begin{bmatrix} -c_1 \\ -c_2 \\ f_{21} \\ 0 \end{bmatrix}, \tag{12}$$

where $a_i = \sqrt{\frac{s}{\kappa_i}}$, $b_i = a_i L$, $c_i = \frac{G_i}{s}$, $d_i = e^{b_i} (i = 1, 2)$, and $f_{21} = \kappa_2 c_2 - \kappa_1 c_1$.

Solution of the linear system (12) yields these coefficients. For the sake of simplicity we assume that each branch in the 3-terminal interconnect tree has the same diffusivity, i.e., $\kappa_1 = \kappa_2 = \kappa$. In order to ensure that this assumption is met, the temperature for each branch should be kept the same due to the fact that the diffusion coefficient in metal (Cu) lines depends on the temperature. With this assumption, we can conclude that $a_1 = a_2 = a$, $b_1 = b_2 = b$, and $d_1 = d_2 = d$. Thus, solving the linear system (12) yields

$$\begin{aligned} A_{1,I} &= \frac{2c_1 d^{-3} - (c_1 - c_2)d^{-2} - 2c_2 d^{-1} - (c_1 - c_2)}{2a(1 - d^{-4})}, \\ B_{1,I} &= \frac{-(c_1 - c_2)d^{-4} - 2c_2 d^{-3} - (c_1 - c_2)d^{-2} + 2c_1 d^{-1}}{2a(1 - d^{-4})}, \\ A_{2,I} &= \frac{-(c_1 - c_2)d^{-4} + 2c_1 d^{-3} - (c_1 - c_2)d^{-2} - 2c_2 d^{-1}}{2a(1 - d^{-4})}, \\ B_{2,I} &= \frac{-2c_2 d^{-3} - (c_1 - c_2)d^{-2} + 2c_1 d^{-1} - (c_1 - c_2)}{2a(1 - d^{-4})}. \end{aligned} \tag{13}$$

In order to derive the analytical solutions $\sigma_1(x,t)$ and $\sigma_2(x,t)$ from (10) and (13) by using the inverse Laplace transform technique, we need to introduce the following functions

$$\begin{aligned} &\xi_1(x,n) = (3+4n)L - x,\ \xi_2(x,n) = (2+4n)L - x, \\ &\xi_3(x,n) = (1+4n)L - x,\ \xi_4(x,n) = 4nL - x, \\ &\xi_5(x,n) = (4+4n)L + x,\ \xi_6(x,n) = (3+4n)L + x, \\ &\xi_7(x,n) = (2+4n)L + x,\ \xi_8(x,n) = (1+4n)L + x, \\ &\eta_1(x,n) = (4+4n)L - x,\ \eta_2(x,n) = (3+4n)L - x, \\ &\eta_3(x,n) = (2+4n)L - x,\ \eta_4(x,n) = (1+4n)L - x, \\ &\eta_5(x,n) = (3+4n)L + x,\ \eta_6(x,n) = (2+4n)L + x, \\ &\eta_7(x,n) = (1+4n)L + x,\ \eta_8(x,n) = 4nL + x, \end{aligned} \tag{14}$$

where n is a nonnegative integer. Also we need to introduce the complementary error function which is defined as

$$\texttt{erfc}\{x\} = \frac{2}{\sqrt{\pi}} \int_x^{+\infty} e^{-t^2} dt. \tag{15}$$

Based on the above complementary error function, we construct the following basis function

$$g(x,t) = 2\sqrt{\frac{\kappa t}{\pi}} e^{-\frac{x^2}{4\kappa t}} - x \times \texttt{erfc}\{\frac{x}{2\sqrt{\kappa t}}\}. \tag{16}$$

Using these functions $\xi_i(x,n)$, $\eta_i(x,n) (i = 1, 2, \ldots, 8)$ and $g(x,t)$, we can obtain the exact analytical solutions for the stress evolution in both segments:

$$\begin{aligned} \sigma_{1,I}(x,t) = \frac{1}{2} \sum_{n=0}^{+\infty} &\{2G_1 g(\xi_1,t) + (G_2 - G_1) g(\xi_2,t) \\ &- 2G_2 g(\xi_3,t) + (G_2 - G_1) g(\xi_4,t)\} \\ + \frac{1}{2} \sum_{n=0}^{+\infty} &\{(G_2 - G_1) g(\xi_5,t) - 2G_2 g(\xi_6,t) \\ &+ (G_2 - G_1) g(\xi_7,t) + 2G_1 g(\xi_8,t)\}, \end{aligned} \tag{17}$$

$$\begin{aligned} \sigma_{2,I}(x,t) = \frac{1}{2} \sum_{n=0}^{+\infty} &\{(G_2 - G_1) g(\eta_1,t) + 2G_1 g(\eta_2,t) \\ &+ (G_2 - G_1) g(\eta_3,t) - 2G_2 g(\eta_4,t)\} \\ + \frac{1}{2} \sum_{n=0}^{+\infty} &\{-2G_2 g(\eta_5,t) + (G_2 - G_1) g(\eta_6,t) \\ &+ 2G_1 g(\eta_7,t) + (G_2 - G_1) g(\eta_8,t)\}. \end{aligned} \tag{18}$$

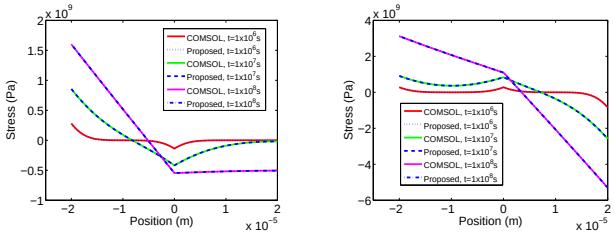

(a) (b)

Fig. 4. The EM stress development along the lines 1 and 2 in the 3-terminal interconnect tree: (a) $j_1 = 2 \times 10^{10} A/m^2$, $j_2 = 0 A/m^2$; (b) $j_1 = 2 \times 10^{10} A/m^2$, $j_2 = 6 \times 10^{10} A/m^2$.

As it will be shown bellow, if we keep the first dominant term ($n = 0$), the error is just about 4%. The approximate solutions with only one dominant term for the segments 1 and 2 are:

$$\begin{aligned} \sigma_{1,I}(x,t) \approx \frac{1}{2} &\{2G_1 g(\xi_1(x,0),t) + (G_2 - G_1) g(\xi_2(x,0),t) \\ &- 2G_2 g(\xi_3(x,0),t) + (G_2 - G_1) g(\xi_4(x,0),t)\} \\ + \frac{1}{2} &\{(G_2 - G_1) g(\xi_5(x,0),t) - 2G_2 g(\xi_6(x,0),t) \\ &+ (G_2 - G_1) g(\xi_7(x,0),t) + 2G_1 g(\xi_8(x,0),t)\}, \end{aligned} \tag{19}$$

$$\begin{aligned} \sigma_{2,I}(x,t) \approx \frac{1}{2} &\{(G_2 - G_1) g(\eta_1(x,0),t) + 2G_1 g(\eta_2(x,0),t) \\ &+ (G_2 - G_1) g(\eta_3(x,0),t) - 2G_2 g(\eta_4(x,0),t)\} \\ + \frac{1}{2} &\{-2G_2 g(\eta_5(x,0),t) + (G_2 - G_1) g(\eta_6(x,0),t) \\ &+ 2G_1 g(\eta_7(x,0),t) + (G_2 - G_1) g(\eta_8(x,0),t)\}. \end{aligned} \tag{20}$$

Fig. 4(a) shows obtained evolution of the stress distribution along the 3-terminal interconnect tree. Analytical solution obtained with the proposed method fits well to the results of the numerical simulation at every time instance. In this case, the segment 1 (left) is called *reservoir* as it supplies atoms to the segment 2 (right), which is called *sink*, [21]. Typically when the current in the sink is zero or small, voids are only nucleated in the reservoir. This is clarified in Fig. 4(a), since the tensile stresses are generated in the reservoir only. But, when the sink becomes active (loaded with nonzero current),

0278-0070 (c) 2015 IEEE. Personal use is permitted, but republication/redistribution requires IEEE permission. See http://www.ieee.org/publications_standards/publications/rights/index.html for more information.

This article has been accepted for publication in a future issue of this journal, but has not been fully edited. Content may change prior to final publication. Citation information: DOI 10.1109/TCAD.2016.2523898, IEEE Transactions on Computer-Aided Design of Integrated Circuits and Systems

voids can be nucleated in the sink as well. In this case, the stress in some portions of the sink may exceed the critical stress that can explain the experimental observation described in [25].

Similar to the single wire case, if the critical stress σ_{crit} is known, then the void nucleation time t_{nuc} can be calculated for each segment:

$$\begin{aligned}\sigma_{1,I}(x, t_{nuc,1}) &= \sigma_{crit},\\ \sigma_{2,I}(x, t_{nuc,2}) &= \sigma_{crit}.\end{aligned} \tag{21}$$

Since $\sigma_{1,I}(x, t_{nuc,1})$ and $\sigma_{2,I}(x, t_{nuc,2})$ are nonlinear functions, an iterative method can be used to find the t_{nuc}. In practical computation of the void nucleation time t_{nuc}, the complementary function can be approximated as $\texttt{erfc}\{x\} \approx \frac{e^{-x^2}}{\sqrt{\pi}x}(1 - \frac{1}{2x^2})$. Substituting this approximate form into the basis function (16), we obtain

$$g(x,t) \approx \frac{4\kappa t}{x^2}\sqrt{\frac{\kappa t}{\pi}}e^{-\frac{x^2}{4\kappa t}}. \tag{22}$$

Thus, a simplified formula for calculating the void nucleation time can be obtained from (19)-(22). Based on this simplified form, the void nucleation time can be computed by using Newton's iterative method with an initial guess which is close to the true value. Figs. 4(a) and 4(b) indicate that the initial estimate can be set to be about 10^7s, which can lead to a much faster convergence.

B. T-shaped 4-terminal interconnect tree

The structure of the T-shaped 4-terminal interconnect tree is shown in Fig. 5. In this case, we have three segments which connect through the middle node "o". The stress evolution equations for this interconnect tree consisting of three lines with the corresponding boundary and initial conditions can be solved. The dynamic stress evolution equation with BC for the T-shaped 4-terminal interconnect tree can be found in the appendix. To calculate the exact analytical solutions by using the Laplace transform technique, we need to assume that every branch in this interconnect tree has the same temperature. The details for deriving the analytical solutions has been given in the appendix and here we only show the final results.

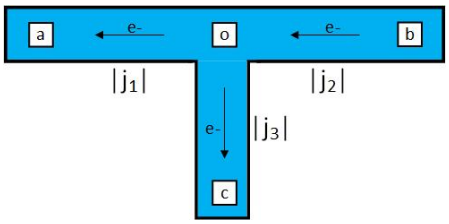

Fig. 5. The T-shaped 4-terminal interconnect tree.

As it was done in the previous case of the two-terminal stress, the analytical solution is represented in terms of a set of auxiliary basis functions by using the complementary error function. Practical calculation formulas should be developed for the exact series solutions of the 4-terminal interconnect

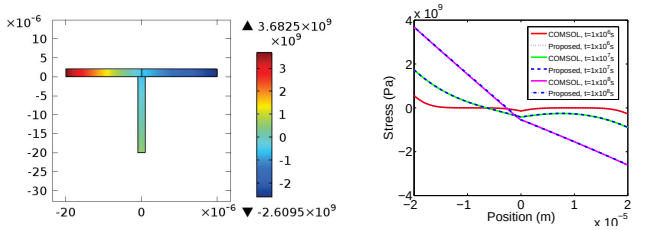

(a) (b)

Fig. 6. (a) The EM stress distribution in the T-shaped 4-terminal wires at the time $t = 1 \times 10^8 s$; (b) the EM stress development along the lines 1 and 2: $j_1 = 4 \times 10^{10} A/m^2$, $j_2 = 2 \times 10^{10} A/m^2$, $j_3 = 1 \times 10^{10} A/m^2$.

tree. Below we will demonstrate that the first dominant term is a good approximate solution:

$$\begin{aligned}\sigma_{1,T}(x_1,t) \approx -\frac{1}{3}\{&-3G_1 g(\xi_1(x_1,0),t) + (G_1 - G_2\\ &+ G_3)g(\xi_2(x_1,0),t) + (G_1 + 2G_2 - 2G_3)g(\xi_3(x_1,0),t)\\ &+ (G_1 - G_2 + G_3)g(\xi_4(x_1,0),t)\} - \frac{1}{3}\{(G_1 - G_2\\ &+ G_3)g(\xi_5(x_1,0),t) + (G_1 + 2G_2 - 2G_3)g(\xi_6(x_1,0),t)\\ &+ (G_1 - G_2 + G_3)g(\xi_7(x_1,0),t) - 3G_1 g(\xi_8(x_1,0),t)\},\end{aligned} \tag{23}$$

$$\begin{aligned}\sigma_{2,T}(x_2,t) \approx -\frac{1}{3}\{&(G_1 - G_2 + G_3)g(\eta_1(x_2,0),t)\\ &- (2G_1 + G_2 + 2G_3)g(\eta_2(x_2,0),t) + (G_1 - G_2 + G_3)\\ &\times g(\eta_3(x_2,0),t) + 3G_2 g(\eta_4(x_2,0),t) - \frac{1}{3}\{3G_2\\ &\times g(\eta_5(x_2,0),t) + (G_1 - G_2 + G_3)g(\eta_6(x_2,0),t)\\ &- (2G_1 + G_2 + 2G_3)g(\eta_7(x_2,0),t)\\ &+ (G_1 - G_2 + G_3)g(\eta_8(x_2,0),t)\},\end{aligned} \tag{24}$$

$$\begin{aligned}\sigma_{3,T}(x_3,t) \approx -\frac{1}{3}\{&-3G_3 g(\xi_1(x_3,0),t) + (G_1 - G_2 + G_3)\\ &\times g(\xi_2(x_3,0),t)(-2G_1 + 2G_2 + G_3)g(\xi_3(x_3,0),t) + (G_1\\ &- G_2 + G_3)g(\xi_4(x_3,0),t)\} - \frac{1}{3}\{(G_1 - G_2 + G_3)\\ &\times g(\xi_5(x_3,0),t) + (-2G_1 + 2G_2 + G_3)g(\xi_6(x_3,0),t)\\ &+ (G_1 - G_2 + G_3)g(\xi_7(x_3,0),t) - 3G_3 g(\xi_8(x_3,0),t)\}.\end{aligned} \tag{25}$$

The void nucleation time t_{nuc} can be obtained by solving the equations $\sigma_{1,T}(x_1, t_{nuc,1}) = \sigma_{crit}$, $\sigma_{2,T}(x_2, t_{nuc,2}) = \sigma_{crit}$, and $\sigma_{3,T}(x_3, t_{nuc,3}) = \sigma_{crit}$. Fig. 6(a) demonstrates the stress distributions in the T-shaped tree shown in Fig. 5 that were obtained with COMSOL. Fig. 6(b) shows an evolution of the stress distributions along the segments 1 and 2 of the T-shaped tree that was obtained with COMSOL and the one-term approximation. Its comparison confirms that the one-term approximation is pretty accurate.

It should be noted that, in a case when the passive reservoir is present (dangling limb), then the corresponding continuity equation will have just stress gradient flux. For the upstream via (the test line is on a higher metal level compared to the current supply line) an ideal description should be modeled as a T-junction represented by a via-body (vertical segment) with the flux-divergence BC, a passive limb (left metal recess), and metal line on the right-hand side. The downstream via (test line is on a lower metal layer compared to the current supply line) can be represented just as a line edge with the flux-divergence BC.

0278-0070 (c) 2015 IEEE. Personal use is permitted, but republication/redistribution requires IEEE permission. See http://www.ieee.org/publications_standards/publications/rights/index.html for more information.

This article has been accepted for publication in a future issue of this journal, but has not been fully edited. Content may change prior to final publication. Citation information: DOI 10.1109/TCAD.2016.2523898, IEEE Transactions on Computer-Aided Design of Integrated Circuits and Systems

C. Cross-shaped 5-terminal interconnect tree

In the cross-shaped 5-terminal interconnect tree shown in Fig. 7 there are four segments which connect to each other through the middle node "o". The exact analytical solution of the stress evolution equation with the corresponding boundary and initial conditions can be obtained. The details for the mathematical derivation of the analytical EM analysis for this 5-terminal interconnect tree can be found in the appendix. Here we only show the final results.

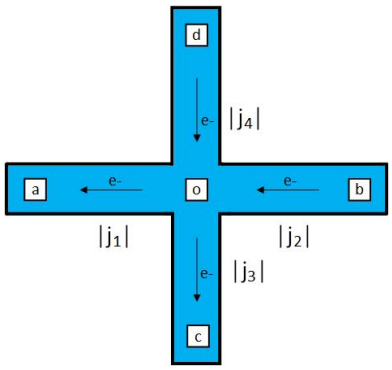

Fig. 7. The cross-shaped 5-terminal interconnect tree.

Again, the approximate solution using the first slow-decaying dominant term for every branch in the cross-shaped tree provides

$$\sigma_{1,+}(x_1,t) \approx -\frac{1}{4}\{-4G_1 g(\xi_1(x_1,0),t) + (G_1 - G_2 + G_3 - G_4)g(\xi_2(x_1,0),t) + 2(G_1 + G_2 - G_3 + G_4)g(\xi_3(x_1,0),t) + (G_1 - G_2 + G_3 - G_4)g(\xi_4(x_1,0),t)\} - \frac{1}{4}\{(G_1 - G_2 + G_3 - G_4)g(\xi_5(x_1,0),t) + 2(G_1 + G_2 - G_3 + G_4) \times g(\xi_6(x_1,0),t) + (G_1 - G_2 + G_3 - G_4)g(\xi_7(x_1,0),t) - 4G_1 g(\xi_8(x_1,0),t)\}, \tag{26}$$

$$\sigma_{2,+}(x_2,t) \approx -\frac{1}{4}\{(G_1 - G_2 + G_3 - G_4)g(\eta_1(x_2,0),t) - 2(G_1 + G_2 + G_3 - G_4)g(\eta_2(x_2,0),t) + (G_1 - G_2 + G_3 - G_4)g(\eta_3(x_2,0),t) + 4G_2 g(\eta_4(x_2,0),t)\} - \frac{1}{4}\{4G_2 \times g(\eta_5(x_2,0),t) + (G_1 - G_2 + G_3 - G_4)g(\eta_6(x_2,0),t) - 2(G_1 + G_2 + G_3 - G_4)g(\eta_7(x_2,0),t) + (G_1 - G_2 + G_3 - G_4)g(\eta_8(x_2,0),t)\}, \tag{27}$$

$$\sigma_{3,+}(x_3,t) \approx -\frac{1}{4}\{-4G_3 g(\xi_1(x_3,0),t) + (G_1 - G_2 + G_3 - G_4)g(\xi_2(x_3,0),t) + 2(-G_1 + G_2 + G_3 + G_4) \times g(\xi_3(x_3,0),t) + (G_1 - G_2 + G_3 - G_4)g(\xi_4(x_3,0),t) - \frac{1}{4}\{(G_1 - G_2 + G_3 - G_4)g(\xi_5(x_3,0),t) + 2(-G_1 + G_2 + G_3 + G_4)g(\xi_6(x_3,0),t) + (G_1 - G_2 + G_3 - G_4) \times g(\xi_7(x_3,0),t) - 4G_3 g(\xi_8(x_3,0),t)\}, \tag{28}$$

$$\sigma_{4,+}(x_4,t) \approx -\frac{1}{4}\{(G_1 - G_2 + G_3 - G_4)g(\eta_1(x_4,0),t) - 2(G_1 - G_2 + G_3 + G_4)g(\eta_2(x_4,0),t) + (G_1 - G_2 + G_3 - G_4)g(\eta_3(x_4,0),t) + 4G_4 g(\eta_4(x_4,0),t) - \frac{1}{4}\{4G_4 \times g(\eta_5(x_4,0),t) + (G_1 - G_2 + G_3 - G_4)g(\eta_6(x_4,0),t) - 2(G_1 - G_2 + G_3 + G_4)g(\eta_7(x_4,0),t) + (G_1 - G_2 + G_3 - G_4)g(\eta_8(x_4,0),t). \tag{29}$$

As before, we can calculate the void nucleation time t_{nuc} by solving the four equations $\sigma_{1,+}(x_1,t_{nuc,1}) = \sigma_{crit}$, $\sigma_{2,+}(x_2,t_{nuc,2}) = \sigma_{crit}$, $\sigma_{3,+}(x_3,t_{nuc,3}) = \sigma_{crit}$, and $\sigma_{4,+}(x_4,t_{nuc,4}) = \sigma_{crit}$.

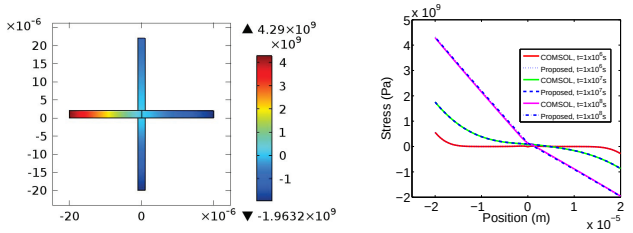

(a) (b)

Fig. 8. (a) The EM stress distribution in the cross-shaped 4-terminal interconnect tree at the time $t = 1 \times 10^8 s$; (b) the EM stress development along the lines 1 and 2: $j_1 = 4 \times 10^{10} A/m^2$, $j_2 = 2 \times 10^{10} A/m^2$, $j_3 = -2 \times 10^{10} A/m^2$, $j_4 = 1 \times 10^{10} A/m^2$.

As an illustration, we set the current densities in the four segments to $j_1 = 4 \times 10^{10} A/m^2$, $j_2 = 2 \times 10^{10} A/m^2$, $j_3 = -2 \times 10^{10} A/m^2 \times 10^{10} A/m^2$, and $j_4 = 1 \times 10^{10} A/m^2$. We use COMSOL to simulate the stress distributions in the cross-shaped tree shown in Fig. 8(a). Stress evolution obtained with our model using the one-term approximation fits well the simulation results obtained with COMSOL, Fig. 8(b).

D. Interconnects with more complex structures

We have derived analytical models for EM reliability analysis in the straight-line 3-terminal interconnect tree, the T-shaped 4-terminal interconnect tree and the cross-shaped 5-terminal interconnect tree, which reflect the practical VLSI interconnect architectures and interconnect layout-design techniques. The effects of temperature, current density and segment length on stress evolution can be easily observed from the proposed analytical models. The developed methodology treats all involved current densities as the effective one. It means that the time-dependent currents are replaced by the effective DC currents, which are calculated on the basis of equal void nucleation times caused by these two currents, [26].

In actual integrated circuits there are various types of interconnect trees as shown in Table II which shows EM-induced reliability models in various studies. Reliability analysis approaches for the straight-line 3-terminal wires, the T-shaped 4-terminal wires and the cross-shaped 5-terminal wires have also been presented in [17] [27] [28]. Experimental characterization for the 3-terminal interconnect tree has been investigated in [17]. A hierarchical reliability methodology for interconnects has been proposed in [27] to calculate time-to-failures which are combined using a joint stochastic model of

0278-0070 (c) 2015 IEEE. Personal use is permitted, but republication/redistribution requires IEEE permission. See http://www.ieee.org/publications_standards/publications/rights/index.html for more information.

This article has been accepted for publication in a future issue of this journal, but has not been fully edited. Content may change prior to final publication. Citation information: DOI 10.1109/TCAD.2016.2523898, IEEE Transactions on Computer-Aided Design of Integrated Circuits and Systems

TABLE II
ELECTROMIGRATION RELIABILITY MODELS IN VARIOUS STUDIES

Ref.	Type of interconnects	Analytic model	Remarks
[11]	2-terminal	Available	EM of confined interconnect lines
[15]	3-terminal	NA	SEM characterization
[17]	3-terminal	NA	Experimental characterization
[19]	3-terminal	NA	L-shaped interconnect tree
[20]	Star-like	Available	Semi-infinite segments
[21]	Multi-terminal	NA	Nodal analysis for electromigration
[27]	Multi-terminal	NA	Hierarchical reliability methodology
[28]	Multi-terminal	NA	Experimental characterization
Proposed	Multi-terminal	Available	Multi-branch interconnect trees

different trees. Experimental characterization of the reliability of Cu dual-damascene interconnect trees with 3-terminal, 4-terminal and 5-terminal configurations has been investigated in [28]. But they did not give a unified analytic form to calculate the stress evolution during the void nucleation phase for these interconnect trees.

It should be noted that while simulation of stress evolution in complex interconnect trees is possible, less computationally intensive analytical models are needed for calculating EM-induced stress evolution. As pointed out in [20], it is impossible to analyze and fabricate all the possible interconnect trees found in an integrated circuit. But we can develop a set of rules and specifications to make realistic reliability assessments of interconnects during the VLSI layout design process. The purpose of our work is to obtain analytical models of EM-induced stress evolution in a multi-branch tree by de-coupling the individual segments through the proper BC accounting the interactions between different branches. The proposed analytical models can also be applied for detailed calculation of the time-dependent stress analysis in the hierarchical reliability methodology for circuit level reliability analysis of interconnects.

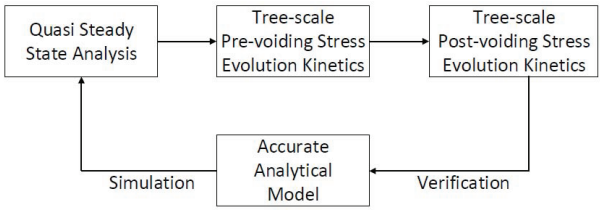

Fig. 9. The EM-related reliability analysis flow based on the analytic model.

In the practical IC design flow, for EM sign-off analysis, the accurate analysis of the stress evolution of multi-branch interconnect trees are first performed for quasi steady state analysis which shows trees with the potential hydrostatic stress larger than the critical stress. Then the tree-scale pre-voiding stress evolution kinetics (the technique proposed in this paper) provides an the exact location and the instance time for the first nucleated void. Then the post-voiding stress evolution kinetics combined with the adjusted current densities everywhere in the tree provides the locations and nucleation times for all other possible voids inside this tree. In the flowchart shown in Fig.9, stress evolution kinetics analyses for multi-branch interconnect trees are fed into accurate analytical models, such as the ones proposed in this paper.

This methodology, which was demonstrated on three different segment configurations, has a general character. It can be implemented in the trees where the "steady-state analysis" shows the locations with the stresses exceeding the critical stress. It will provide an accurate void nucleation time in each tree. These instances in time indicate when the resistances of individual segments start to evolve resulting the current density redistribution. These accurate nucleation times will be used in the EM assessment flow, described in [9], replacing the employed approximation based nucleation times. The post-voiding stress evolution, which is under development now, will allow to predict generation of additional voids in the same interconnect tree, i.e. will lead to more accurate assessment of the evolution of the resistance of interconnect segments, and finally to accurate assessment of IR-drop degradation. As demonstrated in the appendix, the initial problem of solution of the systems of PDEs reduces to solution of the sparse systems of linear algebraic equations. It can be done for any size of the problem. Thus, stress evolution inside interconnect tree of any size can be resolved with required efficiency and accuracy.

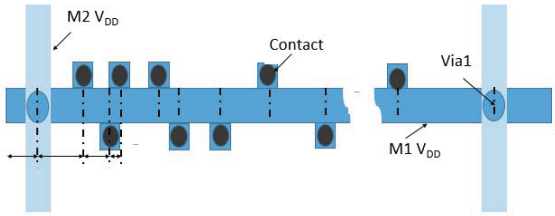

Fig. 10. An example of general realistic interconnect structure.

In order to further illustrate how the analytical model can be extended to a more complex structure, we show an individual interconnect tree of the power delivery grid, as shown in Fig.10. It represents a long metal line with a number of the voltage ports, represented by the vias located at the intersections between power grids (p-g) of the neighboring metal levels, and a much larger number of the current ports, represented by the contacts connecting power grid with the circuits. The latter should be attributed mostly to the trees of the p-g located at the lowest metal level (M1). In general case the V_{DD} M1 power rail is characterized by presence of a large number of the upstream, regarding electron flow, tungsten contacts. V_{SS} rail is stuffed with the downstream tungsten contacts. Due to an extremely low atomic diffusivity of tungsten and, so, a big resistance to EM, the V_{DD} M1 power rail should be more susceptible to EM. Fig.10 shows the schematics of the V_{DD} M1 power rail.

The V_{DD} rail should be divided on the set of segments with the ends represented the voltage and current ports and the ends of the rail. It should be mentioned that due to the very short lengths of the connections between the contact pads and the rail we do not account them in our set up. Stress evolution equations (1) written for each segment and coupled to each other by the BC representing the continuity of stress and fluxes at all junctions should be solved. The general system of equation in this case is a simple n-branch extension of the

0278-0070 (c) 2015 IEEE. Personal use is permitted, but republication/redistribution requires IEEE permission. See http://www.ieee.org/publications_standards/publications/rights/index.html for more information.

This article has been accepted for publication in a future issue of this journal, but has not been fully edited. Content may change prior to final publication. Citation information: DOI 10.1109/TCAD.2016.2523898, IEEE Transactions on Computer-Aided Design of Integrated Circuits and Systems

system (6) written for the case of two connected segments:

$$\begin{aligned}
&\frac{\partial \sigma_1}{\partial t} = \frac{\partial}{\partial x}[\kappa_1(\frac{\partial \sigma_1}{\partial x} + G_1)],\ 0 \le x \le l_1\\
&\frac{\partial \sigma_2}{\partial t} = \frac{\partial}{\partial x}[\kappa_2(\frac{\partial \sigma_2}{\partial x} + G_2)],\ l_1 \le x \le l_2,\\
&\cdots\cdots\\
&\frac{\partial \sigma_{n-1}}{\partial t} = \frac{\partial}{\partial x}[\kappa_{n-1}(\frac{\partial \sigma_{n-1}}{\partial x} + G_{n-1})],\ l_{n-2} \le x \le l_{n-1},\\
&\frac{\partial \sigma_n}{\partial t} = \frac{\partial}{\partial x}[\kappa_n(\frac{\partial \sigma_n}{\partial x} + G_n)],\ l_{n-1} \le x \le L.
\end{aligned} \tag{30}$$

BC for these equations similarly to (7) are the follows:

$$\begin{aligned}
&\kappa_1(\frac{\partial \sigma_1}{\partial x} + G_1) = 0,\ x = 0,\\
&\sigma_1 = \sigma_2,\ x = l_1,\\
&\kappa_1(\frac{\partial \sigma_1}{\partial x} + G_1) = \kappa_2(\frac{\partial \sigma_2}{\partial x} + G_2),\ x = l_1,\\
&\sigma_2 = \sigma_3,\ x = l_2,\\
&\kappa_2(\frac{\partial \sigma_2}{\partial x} + G_2) = \kappa_3(\frac{\partial \sigma_3}{\partial x} + G_3),\ x = l_2,\\
&\cdots\cdots\\
&\kappa_n(\frac{\partial \sigma_n}{\partial x} + G_n) = 0,\ x = L.
\end{aligned} \tag{31}$$

Initial conditions are: $\sigma_i = 0$ at $t = 0$ at all segments. After transforming all the equations and the corresponding BC into Laplace space we get a system of n equations similar to (9) and BC represented by $n+1$ equations similar to (11). Solution of each ODE represented by (10) with two unknown parameters, which will be found from BC, similarly to what was done in the case of two-segments/three terminals case, (13). A problem that we are solving is determination of the moment of time and location on the V_{DD} rail when and where the first void will be nucleated. To do this we do not need to make the inverse Laplace transformation. It is enough to compare the stress in the Laplace space $\sigma_i(x, s)$ with the Laplace transform of the critical stress. It should be also taken into account that not all junctions but just some of them can provide a condition for void nucleation: $\sigma = \sigma_{crit}$. Basically just two types of junctions characterized by specific configurations of the current directions should be considered. First type is the terminating segments serving as the current outlets (electron cathodes), and second the junctions separating two segments with electron flows directed outward this junctions.

IV. Effect of the Segment Length in EM-Induced Stress Evolution

By using the analytical method proposed in Section III, we can obtain closed-form expressions for the EM-induced stress evolution in multi-branch interconnect trees with a variable segment length. This is demonstrated by investigating the effect of segment length on the stress evolution in the straight-line 3-terminal interconnect tree shown in Fig. 11.

Results of the performed analysis are shown in Figs. 12(a)-(d). The directions of the currents in the segments are chosen to be opposite to each other, which causes the tensile stress development at both cathode ends "a" and "b". The stress

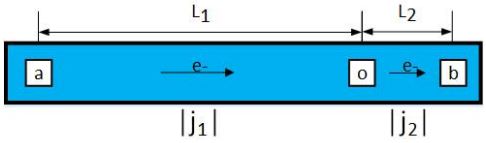

Fig. 11. The straight-line 3-terminal interconnect tree with a variable segment length.

evolution is analyzed with the proposed analytical method. They demonstrate that the decreasing of the length of one of the segments taking place under the fixed electric current load results a progressive development of the compressive stress in this segment. This is caused by a continuously increasing back stress gradient in the short segment due to a continuous supply of atoms from the long segment to the segment boarder. On the other hand, as seen in Fig. 12(c)-(d), a tensile stress can also build up in the right segment if the length of this segment is long enough. By varying the values of the applied current and the segment length one can reach the situation when a void is nucleated first in the short segment.

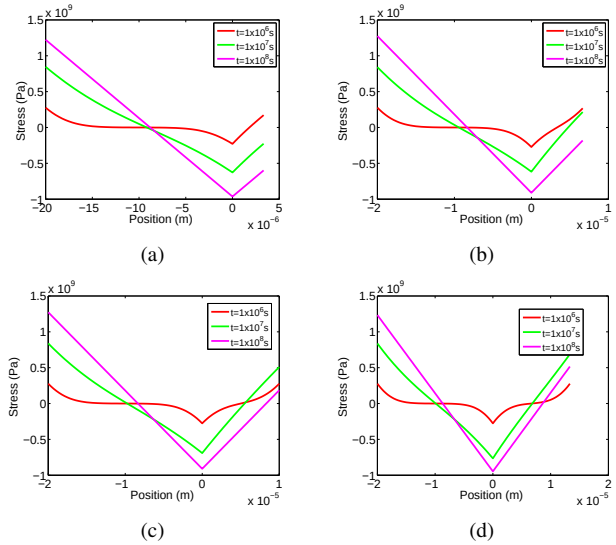

Fig. 12. The EM stress development along the segments 1 and 2 in the three-terminal interconnect tree: (a) $L_2 = \frac{1}{6}L_1$; (b) $L_2 = \frac{2}{6}L_1$; (c) $L_2 = \frac{3}{6}L_1$; (d) $L_2 = \frac{4}{6}L_1$. For call cases: $j_1 = 2{\times}10^{10}A/m^2$, $j_2 = -2{\times}10^{10}A/m^2$.

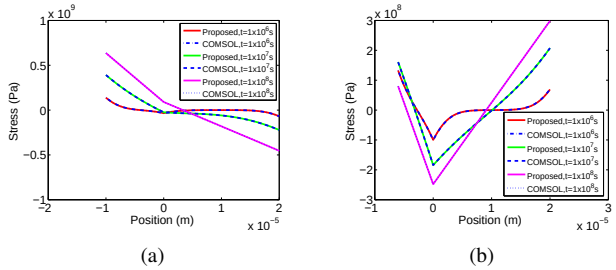

Fig. 13. The EM stress development along the segments 1 and 2 in the three-terminal interconnect tree: (a) $j_1 = 1 \times 10^{10}A/m^2$, $j_2 = 5 \times 10^9 A/m^2$, $L_1 = 10\mu m$, $L_2 = 20\mu m$; (b) $j_1 = 1{\times}10^{10}A/m^2$, $j_2 = -5{\times}10^9 A/m^2$, $L_1 = 6\mu m$, $L_2 = 20\mu m$.

The stress profiles for different times shown in Fig. 13 are

0278-0070 (c) 2015 IEEE. Personal use is permitted, but republication/redistribution requires IEEE permission. See http://www.ieee.org/publications_standards/publications/rights/index.html for more information.

This article has been accepted for publication in a future issue of this journal, but has not been fully edited. Content may change prior to final publication. Citation information: DOI 10.1109/TCAD.2016.2523898, IEEE Transactions on Computer-Aided Design of Integrated Circuits and Systems

obtained from the proposed analytical method and COMSOL simulation. It can be seen from Fig. 13 that the proposed analytical method fits well to the results of the numerical simulations at every time instance. Experimental results show that the proposed analytical method generates very small errors, which is sufficient for practical EM analysis.

V. Experimental Results and Discussions

The proposed dynamic EM model and the method of analysis of multi-branch interconnect trees have been implemented in Matlab and compared with COMSOL, which is considered as a "golden" tool in our work. The material parameters used in our numerical simulations are shown in Table I. Different trees used in our experiment are shown in Figures 3, 5, and 7. The length of each segment was set to $20\mu m$.

A. EM model predictions with different current densities

First, we analyze the EM model predictions against the results of COMSOL simulations using the one term approximation for the cross-shaped 5-terminal interconnect tree. The numerical results for the T-shaped 4-terminal interconnect tree have been discussed in [29]. The EM induced stress distributions of the cross-shaped wire structure (here the only segments 1 and 2 are shown) under different current density sets are shown in Fig. 14(a)-(d). The stress profiles for different times are obtained from the one term approximation of the exact series solution. In the case (a), the stress distribution is similar to the 3-terminal single-wire case where the segment 1 (left) is the *reservoir* and the segment 2 (right) is the active *sink* with small current. Since $j_1 \gg j_2$, the hydrostatic stress in the segment 2 are all compressive (negative). For the case (b), the currents in these segments have different directions. As a result, both of the segments demonstrate tensile stresses, which matches well the results obtained with COMSOL.

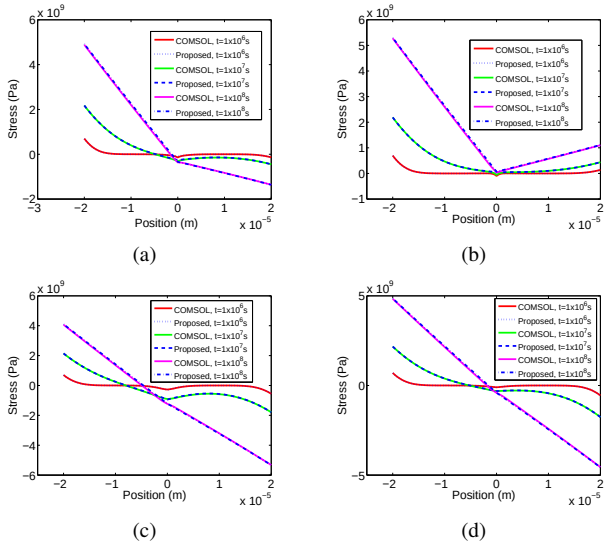

Fig. 14. The EM stress development along the lines 1 and 2 in the cross-shaped 5-terminal interconnect tree: (a) $j_1 = 5 \times 10^{10} A/m^2$, $j_2 = 1 \times 10^{10} A/m^2$, $j_3 = 2.5 \times 10^{10} A/m^2$, $j_4 = 4 \times 10^{10} A/m^2$; (b) $j_1 = 5 \times 10^{10} A/m^2$, $j_2 = -1 \times 10^{10} A/m^2$, $j_3 = -2.5 \times 10^{10} A/m^2$, $j_4 = 4 \times 10^{10} A/m^2$; (c) $j_1 = 5 \times 10^{10} A/m^2$, $j_2 = 4 \times 10^{10} A/m^2$, $j_3 = 3 \times 10^{10} A/m^2$, $j_4 = -5 \times 10^{10} A/m^2$; (d) $j_1 = 5 \times 10^{10} A/m^2$, $j_2 = 4 \times 10^{10} A/m^2$, $j_3 = -3 \times 10^{10} A/m^2$, $j_4 = -5 \times 10^{10} A/m^2$.

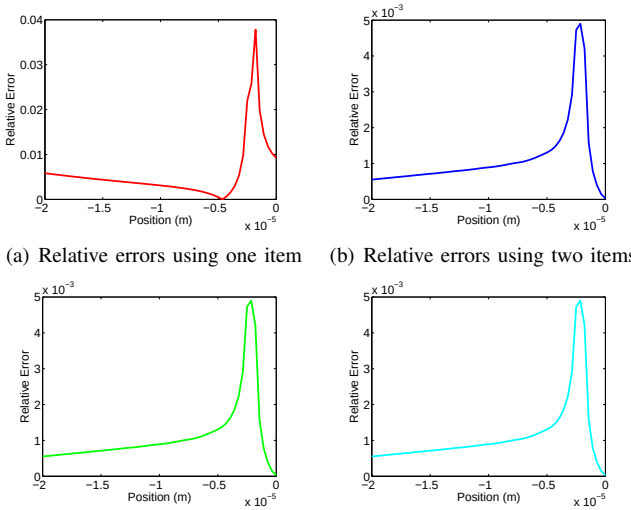

Fig. 15. Relative errors between the proposed analytical model and the COMSOL model for the straight-line 3-terminal interconnect tree: $j_1 = 5 \times 10^{10} A/m^2$, $j_2 = 3 \times 10^{10} A/m^2$.

B. Accuracy study for the compact EM models

Next, we study the accuracy of the EM models employing different number of terms in the exact solution against the COMSOL. Due to limited space, we only show the results for the straight-line 3-terminal interconnect case. We plot the relative errors against COMSOL results for the cases using one term ($n = 0$), two terms ($n = 1$), five terms ($n = 4$) and ten terms ($n = 9$), which are shown in Fig. 15(a)-(d), respectively. As we can see, by using just one term ($n = 0$), we can obtain relative errors less than 4%. By using two terms ($n = 1$), the error is reduced to 0.5%. By using more terms ($n = 4$ and $n = 9$), the errors will still stay around 0.5%, which means that two terms can achieve sufficient accuracy and adding more terms does not increase the accuracy significantly. This is also valid for all other considered interconnect trees.

C. Convergence analysis of the infinite-series solution

To analyze the convergence behavior of the infinite-series solution obtained by the aforementioned method, we need to compare the $(m + l)$-term approximation with the m-term approximation for arbitrary fixed nonnegative integers m and l. Fig. 15(a) illustrates that there are only a few locations in the metal wire where the relative errors stay around 4%. We obtain similar results, when the one-term approximation is applied, for the T-shaped 4-terminal and cross-shaped 5-terminal interconnect trees. It can been observed from Fig. 15(b) that the relative errors using the two-term approximation are just about 0.5%. Therefore, for discussing the convergence behavior of the infinite-series solution to the stress evolution in electromigration reliability analysis, we turn out to compare the one-term approximation with the two-term approximation. This comparison can be seen easily from the numerical simulation results. Fig. 16 shows the comparison

0278-0070 (c) 2015 IEEE. Personal use is permitted, but republication/redistribution requires IEEE permission. See http://www.ieee.org/publications_standards/publications/rights/index.html for more information.

This article has been accepted for publication in a future issue of this journal, but has not been fully edited. Content may change prior to final publication. Citation information: DOI 10.1109/TCAD.2016.2523898, IEEE Transactions on Computer-Aided Design of Integrated Circuits and Systems

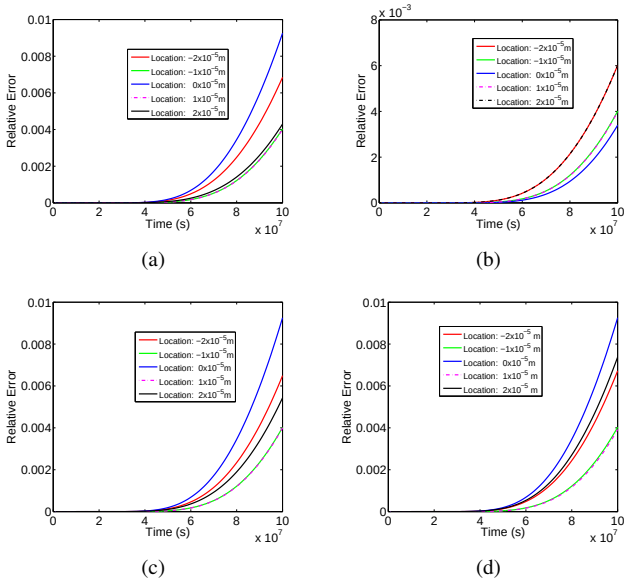

Fig. 16. Relative errors between the one-term and two-term approximations for the cross-shaped 5-terminal wires: (a) $j_1 = 5 \times 10^{10} A/m^2$, $j_2 = 10^{10} A/m^2$, $j_3 = 5 \times 10^{10} A/m^2$, $j_4 = 10^{10} A/m^2$; (b) $j_1 = 5 \times 10^{10} A/m^2$, $j_2 = -10^{10} A/m^2$, $j_3 = -5 \times 10^{10} A/m^2$, $j_4 = 10^{10} A/m^2$; (c) $j_1 = 5 \times 10^{10} A/m^2$, $j_2 = 3 \times 10^{10} A/m^2$, $j_3 = 2 \times 10^{10} A/m^2$, $j_4 = -10^{10} A/m^2$; (d) $j_1 = 5 \times 10^{10} A/m^2$, $j_2 = -3 \times 10^{10} A/m^2$, $j_3 = -2 \times 10^{10} A/m^2$, $j_4 = -10^{10} A/m^2$.

results between the one-term and two-term approximations for the cross-shaped 5-terminal interconnect tree. We can see from Fig. 16 that the relative errors between the one-term and two-term approximations are less than 1%, which shows that the dominant one-term approximation is sufficient for practical EM analysis.

VI. Conclusion

In this paper, we have proposed a new modeling and analysis technique for electromigration reliability analysis in multi-branch interconnect trees, which are common for practical VLSI interconnect architectures and wiring techniques. We have derived the exact analytical solutions to the stress evolution equations for the straight-line 3-terminal wires, the T-shaped 4-terminal wires, and the cross-shaped 5-terminal wires. The new physics-based EM models for multi-branch interconnect trees show an excellent agreement with the detailed numerical analysis. Experimental results showed that using the first dominant basis function can lead to less than 4 % errors. Furthermore, by using the first two basis functions, one can have less than 0.5% errors, which is sufficient for practical EM analysis.

References

[1] B. Bailey, "Thermally challenged," *Semiconductor Engineering*, pp. 1–8, Dec. 2013.

[2] S. Chatterjee, M. B. Fawaz, and F. N. Najm, "Redundancy-aware electromigration checking for mesh power grids," in *IEEE/ACM International Conference on Computer-Aided Design (ICCAD)*, 2013.

[3] V. Mishra and S. S. Sapatnekar, "The impact of electromigration in Copper interconnects on power grid integrity," in *Proc. Design Automation Conf. (DAC)*, June 2013.

[4] I. A. Blech, "Electromigration in thin aluminum films on titanium nitride," *Journal of Applied Physics*, vol. 47, no. 4, pp. 1203–1208, 1976.

[5] J. R. Black, "Electromigration-a brief survey and some recent results," *IEEE Transactions on Electron Devices*, vol. 16, no. 4, pp. 338–347, 1969.

[6] J. R. Lloyd, "New models for interconnect failure in advanced IC technology," in *International Symposium on the Physical and Failure Analysis of Integrated Circuits*, pp. 1–7, 2008.

[7] M. Hauschildt, C. Hennesthal, G. Talut, O. Aubel, M. Gall, K. B. Yeap, and E. Zschech, "Electromigration early failure void nucleation and growth phenomena in Cu and Cu(Mn) interconnects," in *IEEE International Reliability Physics Symposium (IRPS)*, pp. 2C.1.1–2C.1.6, 2013.

[8] M. Pathak, J. S. Pak, D. Pan, and S. K. Lim, "Electromigration modeling and full-chip reliability analysis for BEOL interconnect in TSV-based 3D ICs," in *IEEE/ACM International Conference on Computer-Aided Design (ICCAD)*, pp. 555–562, 2011.

[9] X. Huang, T. Yu, V. Sukharev, and S. X.-D. Tan, "Physics-based electromigration assessment for power grid networks," in *Proc. Design Automation Conf. (DAC)*, June 2014.

[10] V. Sukharev, "Beyond Black's equation full-chip EM/SM assessment in 3D IC stack," *Microelectronic Engineering*, vol. 120, pp. 99–105, May 2014.

[11] M. A. Korhonen, P. Borgesen, K. N. Tu, and C. Y. Li, "Stress evolution due to electromigration in confined metal lines," *Journal of Applied Physics*, vol. 73, no. 8, pp. 3790–3799, 1993.

[12] V. Sukharev, A. Kteyan, E. Zschech, and W. D. Nix, "Microstructure effect on EM-induced degradations in dual inlaid Copper interconnects," *IEEE Transactions on Device and Materials Reliability*, vol. 9, no. 1, pp. 87–97, 2009.

[13] "Comsol multiphysics." http://www.comsol.com.

[14] S. P. Hau-Riege and C. V. Thompson, "Experimental characterization and modeling of the reliability of interconnect trees," *Journal of Applied Physics*, vol. 89, pp. 601–609, January 2001.

[15] A. V. Vairagar, S. G. Mhaisalkar, M. A. Meyer, E. Zschech, A. Krishnamoorthy, K. N. Tu, and A. M. Gusak, "Direct evidence of electromigration failure mechanism in dual-damascene Cu interconnect tree structures," *Applied Physics Letters*, vol. 87, pp. 081909–1–081909–4, August 2005.

[16] C. Thompson, S. Hau-Riege, and V. Andleigh, "Modeling and experimental characterization of electromigration in interconnect trees," in *AIP Conference Proceedings*, pp. 62–73, 1999.

[17] C. L. Gan, C. V. Thompson, K. L. Pey, and W. K. Choi, "Experimental characterization and modeling of the reliability of three-terminal dual-damascene Cu interconnect trees," *Journal of Applied Physics*, vol. 94, pp. 1222–1228, July 2003.

[18] S. M. Alam, *Design Tool and Methodologies for Interconnect Reliability Analysis in Integrated Circuits*. PhD thesis, Massachusetts Institute of Technology, September 2004.

[19] S. P. Hau-Riege and C. V. Thompson, "Electromigration saturation in a simple interconnect tree," *Journal of Applied Physics*, vol. 88, pp. 2382–2385, September 2000.

[20] S. Hau-Riege, *New Methodologies for Interconnect Reliability Assessments of Integrated Circuits*. PhD thesis, Massachusetts Institute of Technology, June 2000.

[21] J. J. Clement, S. P. Riege, R. Cvijetic, and C. V. Thompson, "Methodology for electromigration critical threshold design rule evaluation," *IEEE Trans. on Computer-aid Design of Integrated Circuits and Systems*, vol. 18, no. 5, pp. 576–581, 1999.

[22] A. Abbasinasab and M. Marek-Sadowska, "Blech effect in interconnects: applications and design guidelines," in *International Symposium on Physical Design (ISPD)*, pp. 111–118, 2015.

[23] F. Abraham, *Homogeneous Nucleation Theory*. New York: Academic Press, 1974.

[24] Z. Suo, *Reliability of Interconnect Structures*, vol. 8 of *Comprehensive Structural Integrity*. Amsterdam: Elsevier, 2003.

[25] M. Lin and A. Oates, "An electromigration failure distribution model for short-length conductors incorporating passive sinks/reservoirs," *IEEE Transactions on Device and Materials Reliability*, vol. 13, pp. 322–326, March 2013.

[26] V. Sukharev, X. Huang, and S. X.-D. Tan, "Electromigration induced stress evolution under alternate current and pulse current loads," *Journal of Applied Physics*, vol. 118, pp. 034504–1–034504–10, 2015.

[27] S. Alam, G. Lip, C. Thompson, and D. Troxel, "Circuit level reliability analysis of cu interconnects," in *International Symposium on Quality Electronic Design (ISQED)*, pp. 238–243, 2004.

0278-0070 (c) 2015 IEEE. Personal use is permitted, but republication/redistribution requires IEEE permission. See http://www.ieee.org/publications_standards/publications/rights/index.html for more information.

This article has been accepted for publication in a future issue of this journal, but has not been fully edited. Content may change prior to final publication. Citation information: DOI 10.1109/TCAD.2016.2523898, IEEE Transactions on Computer-Aided Design of Integrated Circuits and Systems

[28] C. Gan, C. Thompson, K. Pey, W. Choi, C. Chang, and Q. Guo, "Experimental characterization of the reliability of multi-terminal dual-damascene copper interconnect trees," in *Materials Research Society Symposium Proceedings (MRSSP)*, pp. 121–126, 2003.

[29] H. Chen, S. X.-D. Tan, V. Sukharev, X. Huang, and T. Kim, "Interconnect reliability modeling and analysis for multi-branch interconnect trees," in *Proc. Design Automation Conf. (DAC)*, June 2015.

VII. Appendix

In this section, we list details for the mathematical derivation of our analytical EM analysis for the T-shaped 4-terminal interconnect tree and the cross-shaped 5-terminal interconnect tree.

A. The complete solutions for the T-shaped 4-terminal interconnect tree

The stress evolution equations for an interconnect tree consisting of three segments

$$\frac{\partial \sigma_1}{\partial t} = \frac{\partial}{\partial x_1}[\kappa_1(\frac{\partial \sigma_1}{\partial x_1} + G_1)], -L < x_1 < 0,\ t > 0,$$
$$\frac{\partial \sigma_2}{\partial t} = \frac{\partial}{\partial x_2}[\kappa_2(\frac{\partial \sigma_2}{\partial x_2} + G_2)], 0 < x_2 < L,\ t > 0,$$
$$\frac{\partial \sigma_3}{\partial t} = \frac{\partial}{\partial x_3}[\kappa_3(\frac{\partial \sigma_3}{\partial x_3} + G_3)], -L < x_3 < 0,\ t > 0,$$

subject to the boundary conditions

$$\kappa_1(\frac{\partial \sigma_1}{\partial x_1} + G_1) = 0,\ \ x_1 = -L,\ t > 0,$$
$$\sigma_1 = \sigma_2 = \sigma_3,\ x_1 = x_2 = x_3 = 0,\ t > 0,$$
$$\kappa_1(\frac{\partial \sigma_1}{\partial x_1} + G_1) - \kappa_2(\frac{\partial \sigma_2}{\partial x_2} + G_2) + \kappa_3(\frac{\partial \sigma_3}{\partial x_3} + G_3) = 0,\ x_1 = x_2 = x_3 = 0,\ t > 0,$$
$$\kappa_2(\frac{\partial \sigma_2}{\partial x_2} + G_2) = 0,\ \ x_2 = L,\ t > 0,$$
$$\kappa_3(\frac{\partial \sigma_3}{\partial x_3} + G_3) = 0,\ \ x_3 = -L,\ t > 0,$$

and the initial conditions

$$\sigma_1(x_1, t) = 0,\ \ -L < x_1 < 0,\ t = 0,$$
$$\sigma_2(x_2, t) = 0,\ \ 0 < x_2 < L,\ t = 0,$$
$$\sigma_3(x_3, t) = 0,\ \ -L < x_3 < 0,\ t = 0.$$

We use the Laplace transform technique to solve the stress evolution equation with given boundary and initial conditions for the T-shaped 4-terminal interconnect tree. By applying the Laplace transform, the analytical solutions in s-domain for each branch can be given as

$$\begin{aligned}\hat{\sigma}_1(x, s) &= A_{1,T} e^{\sqrt{\frac{s}{\kappa_1}}x} + B_{1,T} e^{-\sqrt{\frac{s}{\kappa_1}}x},\\ \hat{\sigma}_2(x, s) &= A_{2,T} e^{\sqrt{\frac{s}{\kappa_2}}x} + B_{2,T} e^{-\sqrt{\frac{s}{\kappa_2}}x},\\ \hat{\sigma}_3(x, s) &= A_{3,T} e^{\sqrt{\frac{s}{\kappa_3}}x} + B_{3,T} e^{-\sqrt{\frac{s}{\kappa_3}}x},\end{aligned} \tag{32}$$

where the coefficients $A_{i,T}$ and $B_{i,T} (i = 1, 2, 3)$ satisfy the linear system (33). Assuming that $\kappa_1 = \kappa_2 = \kappa_3 = \kappa$, then we have $a_1 = a_2 = a_3 = a$, $b_1 = b_2 = b_3 = b$, and $d_1 = d_2 = d_3 = d$. With this assumption, the coefficients $A_{i,T}$ and $B_{i,T}$ can be calculated by (34). By applying the inverse Laplace transformation to $\hat{\sigma}_i(x, s)$ in (32), we can obtain an exact time domain solution

$$\begin{aligned}\sigma_{1,T}(x_1, t) = &-\frac{1}{3}\sum_{n=0}^{+\infty}\{-3G_1 g(\xi_1(x_1, n), t) + (G_1 - G_2 \\ &+ G_3) g(\xi_2(x_1, n), t) + (G_1 + 2G_2 - 2G_3) g(\xi_3(x_1, n), t) \\ &+ (G_1 - G_2 + G_3) g(\xi_4(x_1, n), t)\} - \frac{1}{3}\sum_{n=0}^{+\infty}\{(G_1 - G_2 \\ &+ G_3) g(\xi_5(x_1, n), t) + (G_1 + 2G_2 - 2G_3) g(\xi_6(x_1, n), t) \\ &+ (G_1 - G_2 + G_3) g(\xi_7(x_1, n), t) - 3G_1 g(\xi_8(x_1, n), t)\},\end{aligned}$$

$$\begin{aligned}\sigma_{2,T}(x_2, t) = &-\frac{1}{3}\sum_{n=0}^{+\infty}\{(G_1 - G_2 + G_3) g(\eta_1(x_2, n), t) \\ &- (2G_1 + G_2 + 2G_3) g(\eta_2(x_2, n), t) + (G_1 - G_2 + G_3) \\ &\times g(\eta_3(x_2, n), t) + 3G_2 g(\eta_4(x_2, n), t) - \frac{1}{3}\sum_{n=0}^{+\infty}\{3G_2 \\ &\times g(\eta_5(x_2, n), t) + (G_1 - G_2 + G_3) g(\eta_6(x_2, n), t) \\ &- (2G_1 + G_2 + 2G_3) g(\eta_7(x_2, n), t) \\ &+ (G_1 - G_2 + G_3) g(\eta_8(x_2, n), t)\},\end{aligned}$$

$$\begin{aligned}\sigma_{3,T}(x_3, t) = &-\frac{1}{3}\sum_{n=0}^{+\infty}\{-3G_3 g(\xi_1(x_3, n), t) + (G_1 - G_2 \\ &+ G_3) g(\xi_2(x_3, n), t)(-2G_1 + 2G_2 + G_3) g(\xi_3(x_3, n), t) \\ &+ (G_1 - G_2 + G_3) g(\xi_4(x_3, n), t)\} - \frac{1}{3}\sum_{n=0}^{+\infty}\{(G_1 - G_2 + G_3) \\ &\times g(\xi_5(x_3, n), t) + (-2G_1 + 2G_2 + G_3) g(\xi_6(x_3, n), t) \\ &+ (G_1 - G_2 + G_3) g(\xi_7(x_3, n), t) - 3G_3 g(\xi_8(x_3, n), t)\}.\end{aligned}$$

B. The complete solutions for the cross-shaped 5-terminal interconnect tree

The stress evolution equations for an interconnect tree consisting of four segments

$$\frac{\partial \sigma_1}{\partial t} = \frac{\partial}{\partial x_1}[\kappa_1(\frac{\partial \sigma_1}{\partial x_1} + G_1)],\ -L < x_1 < 0,\ t > 0,$$
$$\frac{\partial \sigma_2}{\partial t} = \frac{\partial}{\partial x_2}[\kappa_2(\frac{\partial \sigma_2}{\partial x_2} + G_2)],\ 0 < x_2 < L,\ t > 0,$$
$$\frac{\partial \sigma_3}{\partial t} = \frac{\partial}{\partial x_3}[\kappa_3(\frac{\partial \sigma_3}{\partial x_3} + G_3)],\ -L < x_3 < 0,\ t > 0,$$
$$\frac{\partial \sigma_4}{\partial t} = \frac{\partial}{\partial x_4}[\kappa_4(\frac{\partial \sigma_4}{\partial x_4} + G_4)],\ 0 < x_4 < L,\ t > 0,$$

0278-0070 (c) 2015 IEEE. Personal use is permitted, but republication/redistribution requires IEEE permission. See http://www.ieee.org/publications_standards/publications/rights/index.html for more information.

This article has been accepted for publication in a future issue of this journal, but has not been fully edited. Content may change prior to final publication. Citation information: DOI 10.1109/TCAD.2016.2523898, IEEE Transactions on Computer-Aided Design of Integrated Circuits and Systems

$$\begin{bmatrix} \frac{a_1}{d_1} & -a_1d_1 & 0 & 0 & 0 & 0 \\ 0 & 0 & a_2d_2 & -\frac{a_2}{d_2} & 0 & 0 \\ 0 & 0 & 0 & 0 & \frac{a_3}{d_3} & -a_3d_3 \\ \kappa_1a_1 & -\kappa_1a_1 & -\kappa_2a_2 & \kappa_2a_2 & \kappa_3a_3 & -\kappa_3a_3 \\ 1 & 1 & -1 & -1 & 0 & 0 \\ 0 & 0 & 1 & 1 & -1 & -1 \end{bmatrix} \begin{bmatrix} A_{1,T} \\ B_{1,T} \\ A_{2,T} \\ B_{2,T} \\ A_{3,T} \\ B_{3,T} \end{bmatrix} = \begin{bmatrix} -c_1 \\ -c_2 \\ -c_3 \\ -\kappa_1c_1 + \kappa_2c_2 - \kappa_3c_3 \\ 0 \\ 0 \end{bmatrix}. \tag{33}$$

$$\begin{aligned} A_{1,T} &= \{3c_1d^{-3} - (c_1 - c_2 + c_3)d^{-2} - (c_1 + 2c_2 - 2c_3)d^{-1} - (c_1 - c_2 + c_3)\}/\{3a(1 - d^{-4})\}, \\ B_{1,T} &= \{-(c_1 - c_2 + c_3)d^{-4} - (c_1 + 2c_2 - 2c_3)d^{-3} - (c_1 - c_2 + c_3)d^{-2} + 3c_1d^{-1}\}/\{3a(1 - d^{-4})\}, \\ A_{2,T} &= \{-(c_1 - c_2 + c_3)d^{-4} + (2c_1 + c_2 + 2c_3)d^{-3} - (c_1 - c_2 + c_3)d^{-2} - 3c_2d^{-1}\}/\{3a(1 - d^{-4})\}, \\ B_{2,T} &= \{-3c_2d^{-3} - (c_1 - c_2 + c_3)d^{-2} + (2c_1 + c_2 + 2c_3)d^{-1} - (c_1 - c_2 + c_3)\}/\{3a(1 - d^{-4})\}, \\ A_{3,T} &= \{3c_3d^{-3} - (c_1 - c_2 + c_3)d^{-2} - (-2c_1 + 2c_2 + c_3)d^{-1} - (c_1 - c_2 + c_3)\}/\{3a(1 - d^{-4})\}, \\ B_{3,T} &= \{-(c_1 - c_2 + c_3)d^{-4} - (-2c_1 + 2c_2 + c_3)d^{-3} - (c_1 - c_2 + c_3)d^{-2} + 3c_3d^{-1}\}/\{3a(1 - d^{-4})\}. \end{aligned} \tag{34}$$

$$\begin{bmatrix} \frac{a_1}{d_1} & -a_1d_1 & 0 & 0 & 0 & 0 & 0 & 0 \\ 0 & 0 & a_2d_2 & -\frac{a_2}{d_2} & 0 & 0 & 0 & 0 \\ 0 & 0 & 0 & 0 & \frac{a_3}{d_3} & -a_3d_3 & 0 & 0 \\ 0 & 0 & 0 & 0 & 0 & 0 & a_4d_4 & -\frac{a_4}{d_4} \\ \kappa_1a_1 & -\kappa_1a_1 & -\kappa_2a_2 & \kappa_2a_2 & \kappa_3a_3 & -\kappa_3a_3 & -\kappa_4a_4 & \kappa_4a_4 \\ 1 & 1 & -1 & -1 & 0 & 0 & 0 & 0 \\ 0 & 0 & 1 & 1 & -1 & -1 & 0 & 0 \\ 0 & 0 & 0 & 0 & 1 & 1 & -1 & -1 \end{bmatrix} \begin{bmatrix} A_{1,+} \\ B_{1,+} \\ A_{2,+} \\ B_{2,+} \\ A_{3,+} \\ B_{3,+} \\ A_{4,+} \\ B_{4,+} \end{bmatrix} = \begin{bmatrix} -c_1 \\ -c_2 \\ -c_3 \\ -c_4 \\ -\kappa_1c_1 + \kappa_2c_2 - \kappa_3c_3 + \kappa_4c_4 \\ 0 \\ 0 \\ 0 \end{bmatrix}. \tag{35}$$

$$\begin{aligned} A_{1,+} &= \{4c_1d^{-3} - (c_1 - c_2 + c_3 - c_4)d^{-2} - (2c_1 + 2c_2 - 2c_3 + 2c_4)d^{-1} - (c_1 - c_2 + c_3 - c_4)\}/\{4a(1 - d^{-4})\}, \\ B_{1,+} &= \{-(c_1 - c_2 + c_3 - c_4)d^{-4} - (2c_1 + 2c_2 - 2c_3 + 2c_4)d^{-3} - (c_1 - c_2 + c_3 - c_4)d^{-2} + 4c_1d^{-1}\}/\{4a(1 - d^{-4})\}, \\ A_{2,+} &= \{-(c_1 - c_2 + c_3 - c_4)d^{-4} + (2c_1 + 2c_2 + 2c_3 - 2c_4)d^{-3} - (c_1 - c_2 + c_3 - c_4)d^{-2} - 4c_2d^{-1}\}/\{4a(1 - d^{-4})\}, \\ B_{2,+} &= \{-4c_2d^{-3} - (c_1 - c_2 + c_3 - c_4)d^{-2} + (2c_1 + 2c_2 + 2c_3 - 2c_4)d^{-1} - (c_1 - c_2 + c_3 - c_4)\}/4a(1 - d^{-4}), \\ A_{3,+} &= \{4c_3d^{-3} - (c_1 - c_2 + c_3 - c_4)d^{-2} - (-2c_1 + 2c_2 + 2c_3 + 2c_4)d^{-1} - (c_1 - c_2 + c_3 - c_4)\}/\{4a(1 - d^{-4})\}, \\ B_{3,+} &= \{-(c_1 - c_2 + c_3 - c_4)d^{-4} - (-2c_1 + 2c_2 + 2c_3 + 2c_4)d^{-3} - (c_1 - c_2 + c_3 - c_4)d^{-2} + 4c_3d^{-1}\}/\{4a(1 - d^{-4})\}, \\ A_{4,+} &= \{-(c_1 - c_2 + c_3 - c_4)d^{-4} + (2c_1 - 2c_2 + 2c_3 + 2c_4)d^{-3} - (c_1 - c_2 + c_3 - c_4)d^{-2} - 4c_4d^{-1}\}/\{4a(1 - d^{-4})\}, \\ B_{4,+} &= \{-4c_4d^{-3} - (c_1 - c_2 + c_3 - c_4)d^{-2} + (2c_1 - 2c_2 + 2c_3 + 2c_4)d^{-1} - (c_1 - c_2 + c_3 - c_4)\}/\{4a(1 - d^{-4})\}. \end{aligned} \tag{36}$$

subject to the boundary conditions

$$\begin{aligned} &\kappa_1(\frac{\partial\sigma_1}{\partial x_1} + G_1) = 0, \ \ x_1 = -L, \ t > 0, \\ &\sigma_1 = \sigma_2 = \sigma_3 = \sigma_4, \ x_1 = x_2 = x_3 = x_4 = 0, \ t > 0, \\ &\kappa_1(\frac{\partial\sigma_1}{\partial x_1} + G_1) - \kappa_2(\frac{\partial\sigma_2}{\partial x} + G_2) \\ &+ \kappa_3(\frac{\partial\sigma_3}{\partial x_3} + G_3) - \kappa_4(\frac{\partial\sigma_4}{\partial x_4} + G_4) = 0, \\ &\qquad x_1 = x_2 = x_3 = x_4 = 0, \ t > 0, \\ &\kappa_2(\frac{\partial\sigma_2}{\partial x_2} + G_2) = 0, \ \ x_2 = L, \ t > 0, \\ &\kappa_3(\frac{\partial\sigma_3}{\partial x_3} + G_3) = 0, \ \ x_3 = -L, \ t > 0, \\ &\kappa_4(\frac{\partial\sigma_4}{\partial x_4} + G_4) = 0, \ \ x_2 = L, \ t > 0, \end{aligned}$$

and the initial conditions

$$\begin{aligned} &\sigma_1(x_1, t) = 0, \ \ -L < x_1 < 0, \ t = 0, \\ &\sigma_2(x_2, t) = 0, \ \ 0 < x_2 < L, \ t = 0, \\ &\sigma_3(x_3, t) = 0, \ \ -L < x_3 < 0, \ t = 0, \\ &\sigma_4(x_4, t) = 0, \ \ 0 < x_4 < L, \ t = 0. \end{aligned}$$

By using the Laplace transform technique, we obtain an exact analytical solution in s-domain

$$\begin{aligned} \hat{\sigma}_1(x, s) &= A_{1,+}e^{\sqrt{\frac{s}{\kappa_1}}x} + B_{1,+}e^{-\sqrt{\frac{s}{\kappa_1}}x}, \\ \hat{\sigma}_2(x, s) &= A_{2,+}e^{\sqrt{\frac{s}{\kappa_2}}x} + B_{2,+}e^{-\sqrt{\frac{s}{\kappa_2}}x}, \\ \hat{\sigma}_3(x, s) &= A_{3,+}e^{\sqrt{\frac{s}{\kappa_3}}x} + B_{3,+}e^{-\sqrt{\frac{s}{\kappa_3}}x}, \\ \hat{\sigma}_4(x, s) &= A_{4,+}e^{\sqrt{\frac{s}{\kappa_4}}x} + B_{4,+}e^{-\sqrt{\frac{s}{\kappa_4}}x}, \end{aligned} \tag{37}$$

where the coefficients $A_{i,+}$ and $B_{i,+}(i = 1, 2, 3, 4)$ can be calculated by solving the linear system (35). Assuming that $\kappa_1 = \kappa_2 = \kappa_3 = \kappa_4 = \kappa$, we have $a_1 = a_2 = a_3 = a$, $b_1 = b_2 = b_3 = b$, and $d_1 = d_2 = d_3 = d$. Thus, the coefficients $A_{i,+}$ and $B_{i,+}$ can be given by (36). By using the inverse Laplace transform technique, we obtain

$$\begin{aligned} \sigma_{1,+}(x_1, t) = &-\frac{1}{4}\sum_{n=0}^{+\infty}\{-4G_1g(\xi_1(x_1, n), t) + (G_1 - G_2 + G_3 \\ &- G_4)g(\xi_2(x_1, n), t) + 2(G_1 + G_2 - G_3 + G_4)g(\xi_3(x_1, n), t) \\ &+ (G_1 - G_2 + G_3 - G_4)g(\xi_4(x_1, n), t)\} - \frac{1}{4}\sum_{n=0}^{+\infty}\{(G_1 - G_2 \\ &+ G_3 - G_4)g(\xi_5(x_1, n), t) + 2(G_1 + G_2 - G_3 + G_4) \\ &\times g(\xi_6(x_1, n), t) + (G_1 - G_2 + G_3 - G_4)g(\xi_7(x_1, n), t) \\ &- 4G_1g(\xi_8(x_1, n), t)\}, \end{aligned}$$

0278-0070 (c) 2015 IEEE. Personal use is permitted, but republication/redistribution requires IEEE permission. See http://www.ieee.org/publications_standards/publications/rights/index.html for more information.

This article has been accepted for publication in a future issue of this journal, but has not been fully edited. Content may change prior to final publication. Citation information: DOI 10.1109/TCAD.2016.2523898, IEEE Transactions on Computer-Aided Design of Integrated Circuits and Systems

$$\sigma_{2,+}(x_2,t) = -\frac{1}{4}\sum_{n=0}^{+\infty}\{(G_1 - G_2 + G_3 - G_4)g(\eta_1(x_2,n),t) - 2(G_1 + G_2 + G_3 - G_4)g(\eta_2(x_2,n),t) + (G_1 - G_2 + G_3 - G_4)g(\eta_3(x_2,n),t) + 4G_2 g(\eta_4(x_2,n),t)\} - \frac{1}{4}\sum_{n=0}^{+\infty}\{4G_2 \times g(\eta_5(x_2,n),t) + (G_1 - G_2 + G_3 - G_4)g(\eta_6(x_2,n),t) - 2(G_1 + G_2 + G_3 - G_4)g(\eta_7(x_2,n),t) + (G_1 - G_2 + G_3 - G_4)g(\eta_8(x_2,n),t)\},$$

$$\sigma_{3,+}(x_3,t) = -\frac{1}{4}\sum_{n=0}^{+\infty}\{-4G_3 g(\xi_1(x_3,n),t) + (G_1 - G_2 + G_3 - G_4)g(\xi_2(x_3,n),t) + 2(-G_1 + G_2 + G_3 + G_4) \times g(\xi_3(x_3,n),t) + (G_1 - G_2 + G_3 - G_4)g(\xi_4(x_3,n),t) - \frac{1}{4}\sum_{n=0}^{+\infty}\{(G_1 - G_2 + G_3 - G_4)g(\xi_5(x_3,n),t) + 2(-G_1 + G_2 + G_3 + G_4)g(\xi_6(x_3,n),t) + (G_1 - G_2 + G_3 - G_4) \times g(\xi_7(x_3,n),t) - 4G_3 g(\xi_8(x_3,n),t)\},$$

$$\sigma_{4,+}(x_4,t) = -\frac{1}{4}\sum_{n=0}^{+\infty}\{(G_1 - G_2 + G_3 - G_4)g(\eta_1(x_4,n),t) - 2(G_1 - G_2 + G_3 + G_4)g(\eta_2(x_4,n),t) + (G_1 - G_2 + G_3 - G_4)g(\eta_3(x_4,n),t) + 4G_4 g(\eta_4(x_4,n),t) - \frac{1}{4}\sum_{n=0}^{+\infty}\{4G_4 \times g(\eta_5(x_4,n),t) + (G_1 - G_2 + G_3 - G_4)g(\eta_6(x_4,n),t) - 2(G_1 - G_2 + G_3 + G_4)g(\eta_7(x_4,n),t) + (G_1 - G_2 + G_3 - G_4)g(\eta_8(x_4,n),t).$$

Hai-Bao Chen received the B.S. degree in information and computing sciences, and the M.S. and Ph.D. degrees in applied mathematics from Xian Jiaotong University, Xian, China, in 2006, 2008, and 2012, respectively. He then joined Huawei Technologies, where he focused on cloud computing and big data. He was a Post-Doctoral Research Fellow with Electrical Engineering Department, University of California, Riverside, Riverside, CA, USA, from 2013 to 2014. He is currently an Assistant Professor in the Department of Micro/Nano-electronics, Shanghai Jiao Tong University, Shanghai, China. His current research interests include model order reduction, system and control theory, circuit simulation, cloud computing and big data, and electromigration reliability. Dr. Chen has authored or co-authored more than 20 papers in scientific journals and conference proceedings. He received one Best Paper Award nomination from Asia and South Pacific Design Automation Conference (ASP-DAC) in 2015.

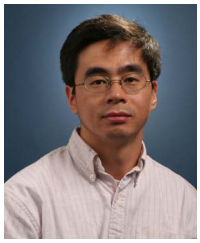

Sheldon X.-D. Tan (S'96-M'99-SM'06) received his B.S. and M.S. degrees in electrical engineering from Fudan University, Shanghai, China in 1992 and 1995, respectively and the Ph.D. degree in electrical and computer engineering from the University of Iowa, Iowa City, in 1999. He is a Professor in the Department of Electrical Engineering, University of California, Riverside, CA. He also is a cooperative faculty member in the Department of Computer Science and Engineering at UCR. He is also a Guest Professor of Shanghai Jiao Tong University and a Guest Professor of University of Electronic Science and Technology of China. His research interests include VLSI reliability modeling, optimization and management at circuit and system levels, thermal modeling, optimization and dynamic thermal management for many-core processors, statistical modeling, simulation and optimization of mixed-signal/RF/analog circuits, parallel circuit simulation techniques based on GPU and multicore systems.

He received Outstanding Oversea Investigator Award from the National Natural Science Foundation of China (NSFC) in 2008. He received NSF CAREER Award in 2004. Dr. Tan received the Best Paper Award from 2007 IEEE International Conference on Computer Design (ICCD'07), the Best Paper Award from 1999 IEEE/ACM Design Automation Conference. He also receives three Best Paper Award Nomination from IEEE/ACM Design Automation Conferences in 2005, 2009 and 2014 and one Best Paper Award nomination from ASPDAC in 2015. He now is serving as the Editor-In-Chief for Integration, The VLSI Journal. He is also serving as an Associate Editor for three journals: IEEE Transaction on VLSI Systems (TVLSI), ACM Transaction on Design Automation of Electronic Systems (TODAE).

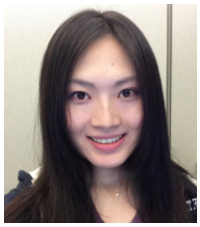

Xin Huang received her B.S. degree from Sichuan University, Chengdu, China in 2008 and the M.S. degree from Peking University, Beijing, China in 2011, both in microelectronics. She is currently working toward the Ph.D. degree in Electrical and Computer Engineering at University of California, Riverside.Her current research interests include electromigration modeling and assessment and reliability-aware performance optimization. Ms. Huang was nominated for the Best Paper Award from 2014 IEEE/ACM Design Automation Conference (DAC2014) and is the inventor of 5 U.S. patents.

Taeyoung Kim received his B.S degree from Konkuk University, Seoul, Korea in 2005 and his M.S. degree in Electrical and Computer Engineering from the University of Virginia in 2012. He is currently a Ph.D. candidate in the Department of Computer Science and Engineering at University of California, Riverside. He is focusing on embedded system design, reliability-aware system modeling and optimization.

Valeriy Sukharev is the Technical Lead of the Design-to-Silicon division of Mentor Graphics Corporation. Dr. Sukharev leads research and development of new full-chip modeling and simulation capabilities for the semiconductor processing and DFM/DFR applications. He has authored and edited a number of books, published more than 100 papers in scientific journals and conference proceedings and holds 20 plus U.S. patents. He has been with Mentor Graphics R&D for seven years. Prior to Mentor Graphics, Dr. Sukharev was a Chief Scientists with Ponte Solutions, Inc., Mountain View, CA, Visiting Professor with Brown University, Providence, RI, and a Guest Researcher with the National Institute of Standards and Technology (NIST), Gaithersburg, MD. He held senior technical positions at LSI Logic Advanced Development Lab, Milpitas, CA. He holds Ph.D. in physical chemistry from the Russian Academy of Sciences.

0278-0070 (c) 2015 IEEE. Personal use is permitted, but republication/redistribution requires IEEE permission. See http://www.ieee.org/publications_standards/publications/rights/index.html for more information.